

to be published in The Astrophysical Journal, Jan 1, 2002

Towards Spectral Classification of L and T Dwarfs: Infrared and Optical Spectroscopy and Analysis

T. R. Geballe¹, G. R. Knapp², S. K. Leggett³, X. Fan⁴, D. A. Golimowski⁵, S. Anderson⁸, J. Brinkmann⁶, I. Csabai^{5,7}, J. E. Gunn², S. L. Hawley⁸, G. Hennessy¹⁰, T. J. Henry⁵, G. J. Hill⁹, R. B. Hindsley¹⁰, Z. Ivezić², R. H. Lupton², A. McDaniel², J. A. Munn¹¹, V. K. Narayanan², E. Peng⁵, J. R. Pier¹¹, C. M. Rockosi¹⁴, D. P. Schneider¹², J. Allyn Smith¹³, M. A. Strauss², Z. I. Tsvetanov⁵, A. Uomoto⁵, D. G. York¹⁴, and W. Zheng⁵

ABSTRACT

We present 0.6–2.5 μm , $R \gtrsim 400$ spectra of twenty-seven cool, low luminosity stars and substellar objects. Based on these and previously published spectra we develop a preliminary spectral classification system for L and T dwarfs. For late L and T types the classification system is based entirely on four spectral indices in the 1–2.5 μm interval. Two of these indices are derived from water absorption bands at 1.15 μm and 1.4 μm , the latter of which shows a smooth increase in depth through the L and T sequences and can be used to classify both spectral types. The other two indices make use of methane absorption features in the H and K bands, with the K band

¹Gemini Observatory, 670 North A'ohoku Place, Hilo, HI 96720

²Princeton University Observatory, Princeton, NJ 08544

³Joint Astronomy Centre, 660 North A'ohoku Place, Hilo, Hawaii 96720

⁴Institute for Advanced Study, Olden Lane, Princeton, NJ 08540

⁵Department of Physics and Astronomy, The Johns Hopkins University, 3701 San Martin Drive, Baltimore, MD 21218, USA

⁶Apache Point Observatory, P.O. Box 59, Sunspot, NM 88349-0059

⁷Department of Physics of Complex Systems, Eötvös University, Pázmány Péter sétány 1/A, Budapest, H-1117, Hungary

⁸University of Washington, Department of Astronomy, Box 351580, Seattle, WA 98195

⁹Department of Astronomy, McDonald Observatory, University of Texas, Austin, TX 78712.

¹⁰U.S. Naval Observatory, 3450 Massachusetts Ave., NW, Washington, DC 20392-5420

¹¹U.S. Naval Observatory, Flagstaff Station, P.O. Box 1149, Flagstaff, AZ 86002-1149

¹²Department of Astronomy and Astrophysics, The Pennsylvania State University, University Park, PA 16802

¹³University of Michigan, Department of Physics, 500 East University, Ann Arbor, MI 48109

¹⁴University of Chicago, Astronomy & Astrophysics Center, 5640 S. Ellis Ave., Chicago, IL 60637

index also applicable to mid to late L dwarfs. Continuum indices shortward of $1 \mu\text{m}$ used by previous authors to classify L dwarfs are found to be useful only through mid L subclasses. We employ the $1.5 \mu\text{m}$ water index and the $2.2 \mu\text{m}$ methane index to complete the L classification through L9.5 and to link the new system with a modified version of the 2MASS “Color-d” index. By correlating the depths of the methane and water absorption features, we establish a T spectral sequence from types T0 to T8, based on all four indices, which is a smooth continuation of the L sequence. We reclassify two 2MASS L8 dwarfs as L9 and L9.5 and identify one SDSS object as L9. In the proposed system methane absorption appears in the K band approximately at L8, two subclasses earlier than its appearance in the H band. The L and T spectral classes are distinguished by the absence and presence, respectively, of H band methane absorption.

Subject headings: brown dwarfs; stars: low mass; spectral types; surveys

1. Introduction

In the last six years, brown dwarfs, objects of mass too low to sustain equilibrium hydrogen burning, have gone from being a theoretical concept with no observed examples to being observationally ubiquitous (Basri 2000). Young brown dwarfs have been discovered in large numbers in star-forming regions (e.g. Hambly et al. 1999; Pinfield et al. 2000; Luhman et al. 2000; Lucas and Roche 2000). Objects with masses ranging from just substellar to those of the Solar System’s giant planets have been found directly or indirectly as companions to nearby stars (Becklin & Zuckerman 1988; Nakajima et al. 1995; Oppenheimer et al. 1995; Mayor & Queloz 1997; Marcy & Butler 1998, 2000; Butler et al. 2000; Marcy, Cochran & Mayor 2000). In addition, large numbers of isolated brown dwarfs have been found in the solar neighborhood (Reid & Hawley 2000; Reid 2001; Kirkpatrick 2001). These observations have led to controversy regarding the distinction between brown dwarfs and planets, with some suggesting that the lower mass limit for brown dwarfs be defined by the ability to burn deuterium (mass greater than $\sim 13 M_J$, Burrows et al 1999), and others preferring the definition that a brown dwarf is any substellar object that forms via the same process as a star (i.e. not from a protoplanetary disk).

Brown dwarfs are of interest in their own right. They have compact structures, low temperatures, and atmospheric constituents that are markedly different from low mass stars. The lowest mass brown dwarfs more closely resemble the gas giant planets than stars, and as such provide insight into the physical and chemical properties of extrasolar giant planets that are at present inaccessible for direct study. After an initial period of deuterium-burning and, for the more massive brown dwarfs, hydrogen-burning, there is no internal energy source and a brown dwarf evolves without reaching thermal equilibrium. This leads to age- and mass-dependent

spectral types, in contrast to main sequence stars, and indeed eventually to effective temperatures lower than that of any stellar photosphere.

It is generally agreed that the very coolest stars and the warmer brown dwarfs ($1300 \text{ K} \lesssim T_{eff} \lesssim 2200 \text{ K}$) require a new spectral class, commonly known as ‘L’ (Martín et al. 1997; Kirkpatrick et al. 1999, hereafter K99) and currently known cooler brown dwarfs ($T_{eff} \lesssim 1300 \text{ K}$), require the addition of an additional class, ‘T’ (K99). The L dwarf sequence is characterized by the disappearance of the red TiO and VO bands from the optical (0.6–1.0 μm) spectrum, the increasing dominance at those wavelengths by broad absorption resonance lines of Na I and K I, and strong H₂O absorption bands and persistent CO overtone bands in the 1–2.5 μm region (Martín et al. 1999, hereafter M99; K99; Kirkpatrick et al. 2000, hereafter K00; Leggett et al. 2001a). In T dwarfs the CO bands are replaced by stronger and more extensive absorptions of CH₄ in the H and K bands, and there is further strengthening of the water bands (Oppenheimer et al. 1995; Geballe et al. 1996; Strauss et al. 1999; Burgasser et al. 1999; Cuby et al. 1999; Tsvetanov et al. 2000). The range of L spectral types has been characterized using optical spectroscopy of objects from the Deep Near-Infrared Survey, DENIS (Delfosse et al. 1997) and the Two Micron All Sky Survey, 2MASS (Skrutskie et al. 1997), while first attempts to describe the range of the ‘T’ spectral sequence are given by Burgasser (2001), Burgasser, Kirkpatrick, & Brown (2001a, hereafter B01a), and by Leggett et al. (2000b, hereafter L00b), whose sample is drawn from the imaging data of the Sloan Digital Sky Survey, SDSS (York et al. 2000). The SDSS imaging data allow the discovery of T dwarfs covering a fairly wide range of spectral characteristics. In pure infrared surveys such as 2MASS, the degeneracy of the colors of T dwarfs with those of stars (see L00b) permits only the latest T dwarfs to be selected readily (without the use of optical photometry).

This paper presents optical (0.6–1.0 μm) and infrared (1.0–2.5 μm) $R \gtrsim 400$ spectroscopy of new L and T dwarfs selected from the SDSS together with new observations of some previously known M, L, and T dwarfs. Following the discovery of transition objects with properties between those of the then known L and T classes (L00b), our goal has been to obtain sufficient spectra of L and T types over the entire 0.6–2.5 μm range and at sufficiently high resolution to allow the continuous characterization of the L and T dwarf spectral sequences. Until now the L sequence has been described only on the basis of optical spectra, and hence it has not been clear if its full extent has been observed. In addition there are significant differences in the assignments of L subclasses for the latest objects (e.g., K99, M99). Using new and previously published spectra, we have devised a set of infrared flux indices from which we have defined a complete L spectral sequence, a T spectral sequence extending to the coolest known brown dwarfs, and a distinct boundary between the L and T sequences. One of the new infrared indices provides a firm link between our L sequence and those proposed by M99 and K99 on the basis of optical spectral indices.

The L and T sequences we have created are purely empirical and the ranges of spectral indices describing them are defined so that they progress smoothly through the known L and T

dwarfs. We have made no attempt to model the spectra or to derive physical quantities such as temperature or mass. Some observational gaps remain in the T sequence, and it is quite likely that the sequence will eventually extend to one or more later subclasses as lower temperature objects are found.

The next two sections describe the selection of objects and the observations. In Section 4 we discuss various indices for spectral typing and present the classification system. Section 5 discusses the results, with emphasis on the definition of the L//T boundary and the link between infrared and optical classification of L dwarfs. The conclusions are given in Section 6. In an adjoining paper, Burgasser et al. (2001b) present an independently derived spectral sequence for T dwarfs, which bears many similarities to the one proposed herein. In a companion paper by Leggett et al. (2001b, hereafter L01b) we provide ZJHKL'M' photometry of many of objects presented herein and we discuss the behavior of broad-band colors as a function of spectral class.

2. The Sample

Our sample consists of the following groups of objects: (1) sixteen dwarfs found in new SDSS imaging data, for which we have obtained the first spectra; (2) two previously reported SDSS dwarfs, one with an incomplete infrared spectrum and one with no reported infrared spectrum; (3) One 2MASS object (also found in the SDSS) with no reported infrared spectrum, (4) eight 2MASS L and T dwarfs for which either only very low resolution ($R \sim 100$) 1–2.5 μm spectra have reported, or there are no reported 1–2.5 μm spectra and our JHK photometry (L01b) suggested that spectroscopy would help maximize the range and completeness of spectral types covered; and (5) fifty-one M, L and T dwarfs for which 1–2.5 μm spectra with $R \gtrsim 400$ have been reported previously. See below and section 3.3 for details of each of these groups. The complete sample is 78 dwarfs covering a range of types from early M to late T and observed at infrared wavelengths using medium spectral resolution and mostly with the same telescope and spectrograph. Optical spectra have been obtained for many of these.

Of the twenty-seven objects whose infrared spectra were observed specifically for the present work, sixteen are newly discovered in the imaging data produced by the SDSS. This sample of SDSS objects is not complete in any way; it was selected to provide as wide as possible range of spectral properties of L and T dwarfs. The SDSS images the sky in five filters (u , g , r , i , z ; Fukugita et al. 1996) covering 0.4–1.0 μm . The magnitudes measured in these filters and quoted in the present paper are denoted by u^* , g^* , r^* , i^* , and z^* , because the SDSS photometric system is not yet finalized. The magnitude scale is on the AB_ν system (J.B. Oke 1969, unpublished), which was updated to the AB_{79} system by Oke and Gunn (1983) and to AB_{95} by Fukugita et al. SDSS photometry is modified from the strict logarithmic magnitude definition to take account of low signal-to-noise ratio, zero, or even negative, measurements (Lupton, Gunn, & Szalay 1999). Data reduction procedures are described by York et al. (2000) and references therein to the SDSS Project Book, and by Lupton et al. (2001). The approximate 5σ detection limits for a point source

observed with a PSF of full width at half maximum of $1''$ is about 22.5 mag in r and i , and about 20.8 mag in z (York et al. 2000). Some sources were only detected in z images, but the i band upper limit indicates that the object is very red. Nearly all of these z -only objects turn out to be false alarms, usually cosmic rays. For the present sample, we required either a 2-sigma detection in the i band and/or a detection by 2MASS (Skrutskie et al 1997) to avoid wasting observing time on spurious images.

Infrared photometry of the new SDSS dwarfs was obtained at the United Kingdom Infrared Telescope (UKIRT), and is reported, along with the SDSS photometry, in Table 1. The photometry of these objects as well as details of the observations are included in L01b. Note that after their first mention in a table or the text, the SDSS and 2MASS object names are abbreviated by the first four digits of the right ascension and first two digits of declination.

Figure 1 shows finding charts, taken from the SDSS z images, for twelve of the sixteen new SDSS objects. Charts for SDSS 0107+00, 0236+00, 0423-04, and 2255-00 are given by Schneider et al. (2002). Figure 2 compares the $i^* - z^*$ colors of the above sample with those of a random sample of 50,000 high-latitude stars extracted from the SDSS imaging data, demonstrating the extreme red colors of the late M, L and T dwarfs. Note that L types tend to have $i^* - z^*$ colors in the range 2–3, whereas for T types the color is usually greater than 3, but that there is apparently significant overlap.

3. Spectroscopy

3.1. Optical

We are engaged in follow-up low-dispersion optical spectroscopy of L and T dwarf candidates selected from the SDSS imaging data, carried out with the Hobby-Eberly Telescope (HET) and Astrophysical Research Consortium (ARC) Telescope. The new observations of twelve of the objects considered in the present paper (eleven SDSS objects and one 2MASS object) are summarized in Table 2. Among the SDSS objects for which we analyze new optical data in this paper are SDSS 0837-00 and SDSS 1021-03, whose infrared spectra were presented by L00b.

The spectra of nine of the objects were obtained using the Double Imaging Spectrograph, DIS, built by J. Gunn, M. Carr and R. Lupton and mounted on the ARC 3.5 m telescope at the Apache Point Observatory. The low-resolution grating with wavelength coverage 5,300–10,000 Å gives a dispersion of 7.1 Å/pixel and a resolution of 14 Å on the red side of the spectrograph. The exposure times were 60 minutes. Spectra of the other three objects were obtained with the Low Resolution Spectrograph LRS (Hill et al. 1998a,b) at the prime focus of the HET (Ramsey et al. 1998). The spectra cover the wavelength range 5100 Å – 9800 Å with a resolution of 20 Å. The exposure times were 60 minutes (for details see Schneider et al. 2002).

Spectra obtained at both telescopes were sky-subtracted and wavelength-calibrated using arc

lamps. Most of the observations were taken under good, although not photometric, atmospheric conditions. Observations of a variety of photometric standard astronomical objects were used for initial flux calibration. The flux scales were adjusted as described below to provide a smooth joining of the optical and infrared spectra.

3.2. New infrared spectra

As indicated in Table 3, most of the new infrared spectra were obtained at UKIRT using CGS4 (Mountain et al. 1990). They were obtained in the J, H and K bands in several observing runs during 2000 and 2001 and, for a small number of objects, also in the UKIRT Z band ($0.85 - 1.05 \mu\text{m}$). The resolution was about 25 \AA in the Z and J bands and 50 \AA in the H and K bands for all of the objects except the bright T dwarf 2MASS 0559-14, for which a spectral resolution of 12.5 \AA in the Z and J bands and 25 \AA in the H and K bands was used. Integration times were 5–45 minutes per band per object.

Wavelength calibration was achieved by obtaining near-simultaneous spectra of arc lamps. Spectra of bright F dwarf stars were recorded immediately prior to or following each spectrum of a candidate brown dwarf. We interpolated the spectra of these stars across strong photospheric features. The spectra of the brown dwarfs were then divided by the interpolated stellar spectra and the result multiplied by a blackbody function corresponding to the temperature of the calibration stars and scaled to the estimated photometric magnitude of the calibration star in the observed infrared band. These procedures remove the effects of telluric absorption, yield the correct broad-band spectral shapes of the target objects, and provide an approximate flux calibration for each band. More accurate flux-calibration was achieved by scaling the spectra to the UKIRT ZJHK photometry presented by L01b (cf. also Table 1).

Some of the new spectra were obtained using the Near-Infrared Spectrometer NIRSPEC (McLean et al. 2000a) on the Keck II telescope on Mauna Kea, Hawaii, in December 2000. They were measured in several filters covering the $0.95-2.5 \mu\text{m}$ band, with spectral resolving powers of ~ 2000 (resolutions of $5-10 \text{ \AA}$). Integration times were 10–40 minute per filter. Data reduction was as described above. To improve the signal-to-noise ratios the NIRSPEC spectra were binned to give resolving powers of ~ 400 . One R ~ 100 Z-band spectrum of one object, SDSS 0207+00, obtained with NSFCAM at the NASA Infrared Telescope Facility (IRTF) on September 23, 2000, is also used in this paper.

In addition to objects selected from the SDSS, we obtained CGS4 spectra of eight 2MASS objects. They are: 2MASS 1523+30 and 2MASS 1632+19, each classified as L8 by K99, 2MASS 0310+16 and 2MASS 0328+23, each classified by K00 as L8 on the basis of Keck LRIS spectra; 2MASS 0559-14, a bright, relatively warm T dwarf whose low resolution infrared spectrum is reported by Burgasser et al. (2000); and 2MASS 1047+21, 2MASS 1217-03, and 2MASS 1225-27, late-type T dwarfs with low resolution infrared spectra reported by Burgasser et

al. (1999) and B01a.

The new infrared observations are summarized in Table 3. The optical observations of most of the objects in this table are listed in Table 2. The optical spectra for 2MASS 0028+15, 2MASS 0328+23, 2MASS 1523+30 and 2MASS 1632+19 were taken from K99 and K00. Optical and infrared spectra were smoothly conjoined by one of several techniques. In some cases they were connected using template objects, i.e. relatively bright objects taken to be representative of the same spectral class. In other cases optical spectra were scaled to be equal in wavelength ranges of overlap with the flux-calibrated infrared spectra. The spectra are displayed in Fig. 3. They are ordered according to the spectral class assigned later in this paper.

3.3. Previously reported spectra

In addition to the twenty-seven objects with newly reported spectra listed in Table 3, we use previously published infrared spectra, mostly obtained by CGS4 on UKIRT, of seven additional SDSS objects: the L5 dwarf SDSS 053951.99-005902.0 (Fan et al. 2000, L00b), the T dwarfs SDSS 0837-00, SDSS 1021-03, and SDSS 125453.90-012247.4 (L00b), SDSS 1326-00 (Fan et al. 2000), SDSS 1346.45-003150.4 (Tsvetanov et al. 2000), and SDSS 162414.37+002915.6 (Strauss et al. 1999). We also use the spectra of M and L dwarfs published by Leggett et al. (2000a, 2001a; see also Kirkpatrick et al. 1995; Ruiz, Allard, & Leggett 1997; Tinney et al. 1998) and the spectra of four dwarfs obtained by Reid et al. (2001; hereafter R01). In the case of 2MASS 031059.9+164816 we have substituted our own spectra in the J and H bands for those obtained by R01. The spectra of other three L dwarfs from R01 (2MASSW J003615.9+182110, 2MASSW J074642.5+200032, and 2MASSW J082519.6+211552) are flux-corrected using the JHK photometry of these objects in L01b. Finally, we utilize the spectra of the T dwarfs Gl 229B (data from Geballe et al. 1996 and Leggett et al. 1999) and Gl 570D (data from Geballe et al. 2001a). The final sample, after classification, consists of 36 M dwarfs, 25 L dwarfs and 17 T dwarfs.

4. Spectral Classification of late L and T Dwarfs

4.1. Previous work and current issues

The recent discoveries of dozens of dwarfs cooler than those of spectral class M, and the large number of high-quality digitized spectra obtained for these dwarfs, have made necessary the extension of the traditional system of stellar spectral classification. Until recently, classification efforts have concentrated mainly on defining late M dwarfs, the M/L transition and a wide range of L dwarfs, using optical spectra. M99, K99, and K00 discuss the classification of objects in this range of spectral types and present spectra and classifications of many tens of objects spanning the stellar-substellar boundary. They characterize and define the range of spectral classes M7 to

L8 (to L6 in the case of M99) by (1) the gradual disappearance of the TiO and VO bands; (2) the increasing depths and breadths of the resonant alkali metal lines and, in particular, several metal hydrides; (3) the increasing depth of the H₂O at 9300 Å band; and (4) the increasing steepness of the 0.6–1.0 μm spectrum. The broadening of the K I lines and the even greater broadening and depth of the Na I D lines at 5889/5896 Å continues into the T dwarf spectra (K99, Liebert et al. 2000), removing much of the optical flux and contributing to the extreme red optical–infrared colors of these objects.

At 1 μm and longward, the M and L dwarfs show strong molecular bands of FeH at 1.00 μm ; H₂O at 1.35–1.50 μm , 1.75–2.05 μm , and longward of 2.3 μm ; and CO at 2.3–2.5 μm ; as well as prominent doublets of K I (Delfosse et al. 1999; McLean et al. 2000b; Leggett et al. 2000a, 2001a) in the J band. The beginning of the T sequence is commonly considered to be marked by the appearance of the CH₄ absorptions at H and K bands. Noll et al. (2000) have shown that the presence of methane is first detectable in the L band via the Q-branch of its fundamental band near 3.3 μm in objects classified optically as about L5, when it is undetectable in the intrinsically weaker shorter wavelength absorption bands. As the L band is much more difficult to observe from the ground than the H and K bands, it does not seem advisable to use the fundamental band for the purpose of classification (L00b, Geballe et al. 2001b).

For T dwarfs the increasing depths of the methane bands in the H window cause a reversal of the trend towards redder $J - H$ colors with later spectral subclass seen in the M and L dwarfs, eventually giving T dwarfs blue $J - H$ values. The same trend reversal is seen in $J - K$, although there the cause appears to be a combination of (1) CH₄, which absorbs flux primarily in the long wavelength half of the band; (2) strong H₂O bands which depress the K-band on both its long and short wavelength edges; and (3) H₂ pressure-induced absorption lines, which depress the entire K band (Borysow, Jørgensen, & Zheng 1997). Some atomic features remain present in T dwarfs and can be seen in Fig. 3. Expanded spectra of the mid-L dwarf SDSS 0107+00 and the mid-T dwarf 2MASS 0559-14 are shown in Fig. 4.

It is generally recognized that the spectral classification of T dwarfs is best made on the basis of 1–2.5 μm spectral behavior rather than that at longer or shorter wavelengths (e.g., B01a). This is because (1) the deep and highly pressure-broadened optical Na I and K I doublets ensure that almost all of the flux from T dwarfs is emitted longward of 1 μm , and (2) for these objects it is easier to obtain high quality spectra at 1–2.5 μm , where a number of molecular bands are prominent, than at longer wavelengths, as discussed above. These characteristics also are true of L subclasses later than about L5, and it can be argued that the classification of L dwarfs later than about L5 also should be made on the basis of 1–2.5 μm spectra.

Tokunaga & Kobayashi 1999, R01, and Testi et al. (2001) have defined sets of indices based largely or entirely on the 1.4 μm and 1.85 μm water bands in order to develop L-dwarf classification schemes that complement existing optical schemes. R01, who analyze medium resolution spectra of eighteen dwarfs, show that their entirely water band-based system is consistent with the

6300–10000 Å system of K99 from spectral types M7 to L8. Testi et al. (2001), who obtained and analyzed low resolution spectra of 26 L dwarfs, find that R01’s indices are less satisfactory than a set of six indices which they devise. None of these indices extend the L sequence beyond L8, the limit of K99’s optical classification scheme. B01a have explored methods of classifying T dwarfs, finding a number of indices that show monotonic and correlated behavior, as well as some indications of photospheric gravity effects that may eventually allow the development of a two-dimensional system.

Whatever spectral signatures are used and wherever the shift is made from indices shortward of 1 μm to ones longward, making a smooth transition from optical to infrared classification poses a potential problem, as does the joining of the L and T sequences. For example, the onset of CH₄ absorption in the H and K bands, clearly the marker of the beginning of the T sequence, may not correspond to a natural “stopping point” in an L sequence defined on the basis of other spectral features in other wavelength bands. These issues are addressed here, but should be revisited as more and better quality spectra both shortward and longward of 1 μm become available.

4.2. Indices and spectral subclasses

We have examined the spectra described in Section 3 with the intent of developing a set of infrared (1.0–2.5 μm) spectral indices that are useful for classifying late L and T dwarfs. We have also reexamined the optical ($< 1 \mu\text{m}$) indices defined by others. The indices to be used should be (1) monotonic and discriminating over large ranges of subclasses, (2) based upon individual spectral features and nearby continua that are unaffected by the behavior of nearby, unrelated spectral features, and (3) useful at sites with reasonable atmospheric transparency and with intermediate-sized telescopes.

We initially considered indices based upon prominent atomic absorption lines longward of 1 μm , but large scatter in the absorption line strengths for late L subclasses preclude their use. For example, the scatter in the strength of the K I doublet at 1.25 μm is easily seen in Fig. 3 and in the data of R01. This scatter is not the result of low quality spectra, but instead may be caused by variations in metallicity, gravity, and/or rotational velocity. Infrared molecular absorption bands offer better possibilities. We also have found that broadband infrared colors (e.g., $J - K$) are not accurate indicators of subclass; reasons for the large amount of scatter in some of them are discussed by L01b.

Table 4 lists eight candidate indices for classifying L and T dwarfs. All the indices are flux ratios, defined by

$$\text{index} = \frac{\int_{\lambda_1}^{\lambda_2} f_\lambda d\lambda}{\int_{\lambda_3}^{\lambda_4} f_\lambda d\lambda} \quad (1)$$

where the wavelength intervals in the numerator and denominator have the same length. The wavelength intervals of the most useful infrared indices are shown in Fig. 4. Scripts for calculating all of the candidate indices are available from SKL on request. Descriptions of the eight indices follow.

- *Three measures of the continuum slope at 0.7–1.0 μm , based on flux ratios of about 0.8 μm to 0.75 μm , 1.0 μm to 0.75 μm , and 1.0 μm to 0.9 μm .* The first of these in Table 4 is the pseudo-continuum (PC3) slope used by M99 and the second is the “Color-d” index defined by K99, modified slightly to avoid the FeH band. The third, based on the continuum slope near 1.0 μm , is our invention, with the wavelength ranges set to exclude the TiO, FeH and metal bands. Both the PC3 and modified Color-d indices show a smooth progression for M dwarfs and early L dwarfs, but both are affected by the broad K I resonance line absorption, which causes the PC3 index to turn over at about L5 and the modified Color-d index to saturate at about L7. The 1.0 μm index defined here shows a large scatter for mid-to-late L types and appears less useful than the other two indices. It may be of some value in classifying T dwarfs. In general, all of the red indices are subject to inaccuracies when applied to substellar objects because of the very low fluxes at those wavelengths.
- *An index to measure the H_2O band at 1.15 μm .* The definition of the 1.2 μm index, which mainly measures the depth of the 1.15 μm band, differs from that used by B01a in that the continuum wavelength range excludes the K I doublet at 1.169 μm . The 1.15 μm H_2O band does not appear until late in the L sequence; prior to that the index mainly reflects the slow reddening of the continuum in the 1.1–1.3 μm interval. It is only suitable for accurate subtyping of the T sequence, where the band strengthens rapidly with later subclass. We compared the 1.2 μm index with a similar 1.1 μm water index, which instead uses the short wavelength continuum peak near 1.08 μm . The latter index shows an increase beginning at spectral class L6, near where the water band first appears. However, there is considerable scatter in the late L – early T range, due to the varying width of the continuum peak (see e.g., Figs. 3b and 3c); because of this it is less effective than the 1.2 μm index.
- *An index to measure the H_2O band at 1.5 μm .* The 1.5 μm index defined here measures the slope of the long wavelength side of the 1.4 μm water band. Its definition is slightly different from that used by R01; the shorter wavelength range is closer to the center of the 1.4 μm feature (but still accessible to ground-based telescopes), and the longer wavelength range better matches the location of the continuum peak as it appears in T dwarfs (see Fig. 4b). It shows a steady increase through both the L and T sequences.
- *An index to measure the H_2O band at 1.9 μm .* Previous attempts to characterize the 1.9 μm H_2O absorption band in L dwarfs have produced mixed results (Tokunaga & Kobayashi 1999; M99; R01; Testi et al. 2001). We have defined a 2.0 μm index that measures the redward slope of the 1.9 μm band while avoiding the strong telluric CO_2 absorptions centered at 2.01 μm and 2.06 μm . Thus, our index resembles that of Testi et al. (2001) but spans a

shorter wavelength range than that of R01. Like Testi et al., we find that this index suffers more scatter than shorter wavelength H_2O indices. Also, the range of this index is more compressed than those of the other water indices. The reason for the relative insensitivity of the $2.0\ \mu\text{m}$ index to spectral subclass is not clear. It is probably not due to continuum emission from dust (Allard et al. 2001; Marley & Ackerman 2001; Burrows et al. 2001, Tsuji 2001), which would dilute the strength of the band, because a similar effect is not seen in the nearby $2.2\ \mu\text{m}$ methane band. We conclude that the $2.0\ \mu\text{m}$ index is not a sufficiently accurate indicator of L or T subclass.

- *Indices for the CH_4 bands at $1.6\ \mu\text{m}$ and $2.2\ \mu\text{m}$.* The definition of the H band methane index differs from that used by B01a; the wavelength range used here includes both the $1.63\ \mu\text{m}$ and $1.67\ \mu\text{m}$ absorption maxima seen in Fig. 4b. The index is flat through the L sequence but increases monotonically through the T sequence. The $2.2\ \mu\text{m}$ index differs from those at similar wavelengths employed by R01 and B01a, and is specifically designed to detect the P branch of the $\nu_2 + \nu_3$ methane band, just longward of the Q branch which produces a narrow absorption feature at $2.20\ \mu\text{m}$ in T dwarfs (Fig. 4b). The $\nu_3 + \nu_4$ and $\nu_1 + \nu_4$ methane bands centered at $2.32\ \mu\text{m}$ and $2.37\ \mu\text{m}$ are somewhat stronger than this band. However, because of the complexity of the spectra of early T dwarfs at $2.3\text{--}2.5\ \mu\text{m}$, with CO, CH_4 , and H_2O all absorbing significantly, the first clear sign of methane in the K band is the appearance of the $2.2\ \mu\text{m}$ band. Although this band of methane does not become obvious until near the L/T boundary, the index we have defined may be of some use for classifying dwarfs as early as L3. For late L subclasses the index is clearly already increasing with spectral subclass, recording an increasing depression of the long wavelength side of the K band, and there is some tendency for this to be occurring at mid L as well.

In summary, we find four indices in the $1.0\text{--}2.5\ \mu\text{m}$ interval which are monotonic over sufficiently wide portions of the L/T sequence that they are suitable for accurately classifying L and T dwarfs. Two of the new indices, at $1.2\ \mu\text{m}$ and $1.5\ \mu\text{m}$, are associated with water absorptions and two, at $1.6\ \mu\text{m}$ and $2.2\ \mu\text{m}$, are associated with methane absorptions. In T dwarfs, all but the H_2O $1.5\ \mu\text{m}$ index measure the actual depths of the associated bands; in the L dwarfs the useful indices measure slopes on the wings of bands (see Fig. 4). Very importantly, the $1.5\ \mu\text{m}$ water band index is suitable for classification across the entire L–T sequence and can be linked to the optical continuum indices PC3 and Color-d, which are already being used for classifying early to mid L types. Although it has a smaller range of usefulness in the L sequence, the $2.2\ \mu\text{m}$ index can be used along with the $1.5\ \mu\text{m}$ index to smoothly link the L and T classifications.

We can now use these infrared indices as well as the PC3 and modified Color-d indices to define numerical ranges for spectral subclasses. This is done in Table 5. In defining the subclasses our intent is: (1) to make the numerical values of the infrared and optical indices in the L0–L5 range generally consistent with existing classifications of M99 and K99 in that range, where the two optical systems agree; (2) to define a sensible L/T boundary and extend the L sequence

smoothly to it; and (3) to define a T sequence, which continues the smooth progression of the indices that are used both for L and T classification and which leaves some room in a system of ten subclasses for as yet undiscovered T dwarfs that are later than any of those currently observed.

4.3. Results

Table 4 lists the spectral indices and derived classifications for all dwarfs in our sample. For each index listed in Table 4, we determined a classification to ± 0.5 subclass based on the definitions in Table 5. We assign a “.5” subclass if the difference of the value of the index and the value at the boundary between subclasses is less than 25% of the range of the index for that subclass, as defined in Table 5. In the final column of the table we have assigned spectral classifications to all L and T objects. These are based on the unweighted averages of the classifications from all six usable optical and infrared indices for L5 and earlier, and on the averages of only the four infrared indices for later objects. The classifications of the M dwarfs in Table 4 are obtained from the literature, except for SDSS 2255-00, which we have classified to be consistent with other late type M dwarfs using the infrared water bands.

Figure 5 contains plots of the observed infrared indices versus final assigned spectral class. A large majority of the data points for each index fall within the defined range for that index, demonstrating the accuracy of the technique. In most cases the L and T classifications are consistent within the overall classification to within about one-half of a subclass and the final classification may be considered accurate to that amount. Larger uncertainties are noted in the last column of Table 4 and several of these cases are discussed in section 5.1.

5. Discussion

5.1. Comparison with previous classifications and internal consistency

Our classifications of L0–L5 dwarfs are in good agreement with those of M99, K99, and K00 and the new infrared indices and the 0.6–1.0 μm continuum indices complement one other in this range of subclasses. Clearly, optical indices should be weighted heavily when classifying such objects. For later L dwarfs, however, the 1.5 μm and 2.2 μm indices yield additional information and are more accurate classification tools than the 0.6–1.0 μm continuum indices. As shown in Table 5 we are unable to define a classification beyond L4 for the PC3 index and beyond L6 for the Color-d index. The dwarfs for which our classifications differ significantly from previously published ones are 2MASS 0028+15, where we obtain L3 whereas K00 find L4.5; 2MASS 0825+21, where we find L6 but K00 and R01 find L7.5; 2MASS 0310+16 and 2MASS 0328+23, which we classify as L9 and L9.5, respectively, whereas K00 obtain L8 for both; and 2MASS 1632+19, which we find to be L7.5, but M99 classify L6. Most of these are late-type L dwarfs, where we expect

larger discrepancies.

We found that the latest L subclasses described both by M99 and K99 correspond fairly closely to the boundary between L and T classes (i.e., to the onset of observable methane absorption in the H and K bands). We also determined that a continued smooth progression of the $1.5 \mu\text{m}$ water band index to this boundary requires several additional L subclasses beyond L5, and hence matches the K99 classification system (L0–L8) better than that of M99 (L0–L6). Therefore, our scheme is loosely correlated with the remainder of the K99 L sequence, with values of both the $1.5 \mu\text{m}$ and $2.2 \mu\text{m}$ indices that roughly match the K99 classifications. However, as discussed above, we found a number of instances in which the values of the two infrared indices implied a different L classification than that provided by K99. In addition, as discussed in section 5.2 below, we define an L9 subclass between L8 and T0. If generally adopted, this might require a reworking of the optical classification systems for the later L subclasses.

For L types where both the $1.5 \mu\text{m}$ and $2.2 \mu\text{m}$ indices are measured, the agreement between them is one subclass or better for 15 of the 23 cases (see Table 4 and Fig. 6). Agreement generally improves with later subclass. There are three instances (GD 165B, DENIS 0205-11, and DENIS 1228-15) for which the two indices give widely discrepant results. The final uncertainties in those cases are ± 2 subclasses (see Table 4); however, in each case our final assignment of spectral class is consistent with K00 and R01. Each of these dwarfs as well as 2MASS 0345+25 is in a closely spaced multiple system (Becklin & Zuckerman 1988; Martín, Brandner, & Basri 1999; Koerner et al. 1999; Reid et al. 1999); perhaps they have additional unseen components which lead to the discrepancies. They are not plotted in Fig. 6.

No detailed classification system for T dwarfs has been proposed previously, although some possibilities have been explored by B01a. Burgasser et al. (2001b) are also suggesting a scheme for T dwarfs, which gives similar results as our system. The latest T dwarfs that we classified are 2MASS 1217-03 and Gl 570D, both T8. The former appears marginally earlier in three of the four infrared indices. The next latest object that we have classified is the T6.5 dwarf 2MASS 1047+21. We have not yet found examples of T5 or T7 dwarfs.

For the T dwarfs the agreement between the four indices we have used for classification is generally better than the agreement for the indices used for the L dwarfs (see Table 4 and Fig. 6). This is because the indices have much wider ranges of values through the T sequence than through the L sequence. A single index usually agrees with the final T spectral classification to ± 0.5 or less. Accuracy of classification increases with later spectral type. Interestingly, the T dwarf with the most uncertain classification in our system is the “prototype,” Gl 229B, assigned T6. Its deviations, which are easily seen in Fig. 5 (the most discrepant points at T6), probably are not intrinsic to Gl 229B, but rather are related to the difficulty in correcting its spectrum for stray and diffracted light from the nearby primary, which is roughly 10,000 times brighter in the *J*, *H*, and *K* bands. Both Gl 229B and SDSS 1624+00 are classified T6, but we note that both Liebert et al. (2000) and Nakajima et al. (2000) find that Gl 229B is cooler, based on the widths and strengths

of atomic lines and its slightly deeper $1.6\text{ }\mu\text{m}$ methane band, from which one might infer that in a different or finer system it might be assigned a later subclass than SDSS 1624+00. Taking our spectra at face value, we find that Gl 229B is later than SDSS 1624+00 in its $1.6\text{ }\mu\text{m}$ methane index, but earlier in its $1.5\text{ }\mu\text{m}$ water and $2.2\text{ }\mu\text{m}$ methane indices.

5.2. The L/T boundary and the T sequence

The numerous spectra of late-L dwarfs and early-T dwarfs permit us to examine in detail the onset of methane absorption in brown dwarf spectra and to propose a boundary between the L and T classes. Figure 7 shows a representative selection of late L and early T spectra in the $1.45\text{--}2.50\text{ }\mu\text{m}$ region, where the critical absorption features and indices are situated. Close examination of these spectra shows that the $2.20\text{ }\mu\text{m}$ methane absorption is first noticeable at spectral subclass L8. The absorption is quite subtle at this subclass, appearing as a slight inflection near $2.20\text{ }\mu\text{m}$. At somewhat later subclasses a flux minimum is seen at that wavelength. The index measuring this feature also measures the slope between $2.1\text{ }\mu\text{m}$ and $2.25\text{ }\mu\text{m}$ changing steadily from mid to late L. H_2 collision-induced absorption is expected to be fairly flat across the K band (Borysow et al. 1997), due to the contributions by several H_2 transitions at different wavelengths in the band and the breadths of each absorption profile, and probably is not responsible for this change. The effect of the $2.20\text{ }\mu\text{m}$ CH_4 absorption is to increase the value of the index; by T3 the CH_4 absorption is very strong.

In contrast, the methane bands at $1.6\text{--}1.7\text{ }\mu\text{m}$ are not seen at subclasses L8 and L9 in our system (see Figs. 4b and 7). The spectra of 2MASS 1523+30 and SDSS 0830+48, which we classify as L8 and L9, respectively, are flat from $1.60\text{ }\mu\text{m}$ to $1.69\text{ }\mu\text{m}$, as are spectra of earlier L subclasses. The two absorption features at $1.67\text{ }\mu\text{m}$ (due to the $2\nu_3$ Q branch) and $1.63\text{ }\mu\text{m}$ are first clearly seen at T0, two subclasses later than where the $2.2\text{ }\mu\text{m}$ ($\nu_2 + \nu_3$) band first becomes apparent. Unlike the K band methane index, the index measuring the $1.6\text{ }\mu\text{m}$ methane bands is only useful for distinguishing T subclasses.

Thus the boundary between L and T classifications in our proposed system corresponds to the appearance of methane absorption in the H band; i.e., to its earliest appearance in *both* the H and K bands. It is this choice of boundary and the maintainance of smoothly varying infrared indices through it that have led us to define an L9 subclass. The proposed L/T boundary is preferred over one defined as the onset of CH_4 absorption in the K band, for several reasons: (1) the noise levels at shorter infrared wavelengths are generally lower than at longer wavelengths; (2) the continuum flux levels of brown dwarfs on the L/T boundary are higher at $1.6\text{ }\mu\text{m}$ than at $2.2\text{ }\mu\text{m}$; and (3) the (later) first appearance of methane in the H band creates a more prominent and obvious spectral feature than the (earlier) appearance in the K band.

Figure 8 shows the spectra of T type dwarfs from T0 through T8, with adjacent spectra spaced by one subclass (except for the gaps between T4.5 and T6 and between T6 and T8). The

spectra show a smooth progression through the sequence, as was the intention when the ranges of indices were designed for each subclass. Note that the $1.5 \mu\text{m}$ index measures the slope of the shoulder of the $1.4 \mu\text{m}$ water band, whereas the other three indices measure the actual depths of the associated features (see Fig. 4). However, it is apparent from Fig. 8, and not surprising, that increasing slope of the shoulders of the $1.4 \mu\text{m}$ water band also corresponds to a steady deepening of that band with later subclass.

5.3. Linking the infrared and optical indices

Figure 9 shows the modified Color-d optical index plotted against the $1.5 \mu\text{m}$ index for all isolated L dwarfs in which both indices were measured. The Color-d index saturates above L6, as illustrated in the figure. For 7 of 8 of the objects in the L0–L6 range the agreement between the two indices is better than one subclass, and in half it is better than one-half subclass. The discrepant object is 2MASS 0036+18, whose Color-d classification is L2.5 and the whose $1.5 \mu\text{m}$ and $2.2 \mu\text{m}$ classifications are L4.5 and L5, respectively. (Note that K00 have classified this object as L3.5 and that our overall classification is L4.) The discrepant case notwithstanding, the good correlation of these indices in the L0–L6 range permits a graceful transition between the optical and infrared classification schemes. More data and further comparison of the $1.5 \mu\text{m}$ index with other optical indices are needed to strengthen this link between the two classification schemes.

6. Conclusions

We have developed a system for classifying L and T dwarfs, based largely on four newly defined spectral indices in the 1.0 – $2.5 \mu\text{m}$ range, and have used it to classify objects from L0 to T8. Two new indices we use are associated with the 1.15 and $1.4 \mu\text{m}$ water bands and two are associated with the 1.65 and $2.2 \mu\text{m}$ methane bands. At L0–L6 the new classification system gives consistent results with the optical systems of M99 and K99, and it appears that they can be accurately aligned using the $1.5 \mu\text{m}$ water and modified Color-d (and possibly other optical) indices. For later L types and all T types, the new indices give satisfactory and self-consistent results. An L classification based on either the $1.5 \mu\text{m}$ or $2.2 \mu\text{m}$ index is usually accurate to within ± 1 subclass, and a T classification using any one of the four infrared indices is usually accurate to within ± 0.5 subclass. The boundary between the L and T classes has been thoroughly investigated. We define the boundary to be the appearance of methane absorption in the H band, which occurs approximately two spectral subclasses after its appearance in the K band.

Spectra of additional L and T dwarfs are needed to refine the definitions of the subclasses. Nevertheless, as defined here the L sequence is complete, extending from L0 to L9.5 and smoothly connecting to the T sequence. The same cannot be said of the T sequence, as objects later than T8, yet to be observed, should exist. Observing the full extent of the T sequence and determining

whether the present classification system is acceptable or requires compression, or a more radical alteration, needs the detection and spectral study of cooler and presumably fainter dwarfs than currently found. The range of effective temperatures of T0-T8 dwarfs is 800–1300 K (Geballe et al. 2001a; L01b). Radical changes in the 1.0–2.5 μm spectrum should not occur until temperatures are low enough that water vapor condenses, probably at $T_{\text{eff}} \sim 500$ K (Marley & Ackerman 2001). Hence, compression of the classification system defined here is a possibility. Finally, clear understandings of the effects of varying gravity, rotation, dust, and metal abundance, and incorporating them into a multi-dimensional classification system will require higher precision and probably higher resolution spectra than reported here, together with accurate model atmospheres and spectra.

We thank the 2MASS group (A. J. Burgasser, J. D. Kirkpatrick, M. E. Brown, I. N. Reid and colleagues) for many valuable discussions on spectral typing, for providing data before publication, and for communicating their spectral sequence for L and T dwarfs before publication. This shared information allowed us to make a consistent first set of T dwarf spectral classifications prior to more detailed analysis. GRK is grateful for support from Princeton University via an Old Dominion Fellowship and from NASA via grants NAG-6734 and NAG5-8083. XF acknowledges supports from NSF grant PHY-0070928 and a Frank and Peggy Taplin Fellowship. DAG acknowledges support from the Center for Astrophysical Sciences at Johns Hopkins University. DPS acknowledges support from NSF grant (NSF99-00703).

The Sloan Digital Sky Survey (SDSS) is a joint project of the University of Chicago, Fermilab, the Institute for Advanced Study, the Japan Participation Group, the Johns Hopkins University, the Max Planck Institute for Astronomy (MPIA), the Max Planck Institute for Astrophysics (MPA), New Mexico State University, Princeton University, the United States Naval Observatory, and the University of Washington. Apache Point Observatory, site of the SDSS telescopes, is operated by the Astrophysical Research Consortium (ARC). Funding for the project has been provided by the Alfred P. Sloan Foundation, the National Science Foundation, the U.S. Department of Energy, the Japanese Monbukagakusho, and the Max Planck Society. The SDSS web site is <http://www.sdss.org/>

UKIRT is operated by the Joint Astronomy Centre on behalf of the UK Particle Physics and Astronomy Research Council. Some of the observations made there were done through the UKIRT Service Program. We thank the staff of UKIRT for its expert help. We also are grateful to the staff of the W.M. Keck Observatory, which is operated as a scientific partnership among the California Institute of Technology, the University of California and the National Aeronautics and Space Administration and was made possible by the generous financial support of the W.M. Keck Foundation. The Hobby-Eberly Telescope (HET) is a joint project of the University of Texas at Austin, the Pennsylvania State University, Stanford University, Ludwig-Maximilians-Universität München, and Georg-August-Universität Göttingen. The HET is named in honor of its principal benefactors, William P. Hobby and Robert E. Eberly.

REFERENCES

Allard, F., Hauschildt, P. H., Alexander, D. R., Tamama, A., & Schweitzer, A. 2001, *ApJ*, 556, 357

Basri, G. 2000, *Scientific American*, 282, 57

Becklin, E. E., & Zuckerman, B. 1988, *Nature*, 336, 656

Borysow, A., Jørgensen, U. G., & Zheng, C. 1997, *A&A*, 324, 185

Burgasser, A. J. et al. 1999, *ApJ*, 522, L65

Burgasser, A. J., et al. 2000, *AJ*, 120, 1100

Burgasser, A. J., 2001, in ‘Galactic Structure, Stars and the Interstellar Medium’, ed. C. Woodward & M. Bicay, *ASP Conf Ser* (in press - astro-ph/0101242)

Burgasser, A. J., Kirkpatrick, J.D., & Brown, M.E., 2001a, in ‘Proceedings of the Meeting on Ultracool Dwarfs’, I.A.U. 24th General Assembly, eds. H.R.A. Jones, M. Gerbaldi, & I.A. Steele (Heidelberg: Springer-Verlag), in press (astro-ph/1010243) (B01a)

Burgasser, A. J., et al. 2001b, *ApJ*, in press

Burrows, A. 1999, in *Planets Outside the Solar System: Theory and Observations*, eds J.-M. Mariotti & D. Alloin (Dordrecht: Kluwer), 121

Burrows, A., Marley, M. S., & Sharp, C. M., 2000, *ApJ*, 531, 438

Burrows, A., Hubbard, W. B., Lunine, J. I., & Liebert, J. 2001, *Rev. Mod. Phys.*, in press (astro-ph/0103383)

Butler, R. P., Vogt, S. S., Marcy, G. W., Fischer, D. A., Henry, G. W., & Apps, K. 2000, *ApJ*, 545, 504

Cuby, J. G., Saracco, P., Moorwood, A. F. M., D’Odorico, S., Lidman, C., Comerón, F., & Spyromilio, J. 1999, *A&A*, 349, L41

Delfosse, X., Tinney, C. G., Forveille, T., Epchtein, N., Borsenberger, J., Fouqué, P., Kimeswenger, S., & Tiphène, D. 1999 *A&AS*, 135, 41

Fan, X., et al. 2000, *AJ*, 119, 928

Fukugita, M., Ichikawa, T., Gunn, J. E., Doi, M., Shimasaku, K., Schneider, D. P 1996, *AJ*, 111, 1748

Geballe, T. R., Kulkarni, S. R., Woodward, C. E., & Sloan, C. G. 1996, *ApJ*, 467, L101

Geballe, T. R., Saumon, D., Leggett, S. K., Knapp, G. R., Marley, M. S., & Lodders, K. 2001a, *ApJ*, 556, 373

Geballe, T. R., Noll, K. S., Leggett, S. K., Knapp, G. R., & Golimowski, D. A. 2001b, in Proceedings of the Meeting on Ultracool Dwarfs, I.A.U. 24th General Assembly, eds. H.R.A. Jones, M. Gerbaldi, & I.A. Steele (Heidelberg: Springer-Verlag), in press

Gunn, J. E., Carr, M. A., Rockosi, C. M., Sekiguchi, M., et al. 1998, *AJ*, 116, 3040

Hambly, N. C., Hodgkin, S. T., Cossburn, M. R., & Jameson, R. F. 1999, *MNRAS*, 303, 835

Hill, G. J., Nicklas, H. E., MacQueen, P. J., Mitsch, W., Wellem, W., Altmann, W., Wesley, G. L., & Ray, F. B. 1998a, *Proc. SPIE* 3335, 433

Hill, G. J., Nicklas, H. E., MacQueen, P. J., Tejada, C., Cobos Duenas, F. J., & Mitsch, W. 1998b, *Proc. SPIE* 3335, 433

Kirkpatrick, J. D. 2001, in Galactic Structure, Stars and the Interstellar Medium, ed. C. Woodward & M. Bicay, *ASP Conf. Ser.*, in press

Kirkpatrick, J. D., Henry, T. J., & Simons, D. A. 1995, *AJ*, 109, 797

Kirkpatrick, J. D., et al. 1999, *ApJ*, 519, 802 (K99)

Kirkpatrick, J. D., et al. 2000, *AJ*, 120, 447 (K00)

Koerner, D. W., Kirkpatrick, J. D., McElwain, M. W., & Bonaventura, N. R. 1999, *ApJ*, 526, 25

Leggett, S.K., Toomey, D.W., Geballe, T.R., & Brown, R.H. 1999, *ApJ*, 517, L139

Leggett, S. K., Allard, F., Dahn, C., Hauschildt, P. H., Kerr, T. H., & Rayner, J. 2000a, *ApJ*, 535, 965

Leggett, S. K., et al. 2000b, *ApJ*, 536, L35 (L00b)

Leggett, S. K., Allard, F., Geballe, T. R., Hauschildt, P. H., & Schweitzer, A. 2001a, *ApJ*, 548, 908

Leggett, S. K., Golimowski, D. A., Fan, X., Geballe, T. R., Knapp, G. R., et al. 2001b, *ApJ*, in press (L01)

Lierbert, J., Reid, I. N., Burrows, A., Burgasser, A. J., Kirkpatrick, J. D., & Gizis, J.E. 2000, *ApJ*, 533, L155

Lucas, P. W. & Roche, P. F. 2000, *MNRAS*, 314, 858

Luhman, K. L., Rieke, G. H., Young, E. T., Cotera, A. S., Chen, H., Rieke, M. J., Schneider, G., & Thompson, R. I. 2000, *ApJ*, 540, 1016

Lupton, R. H., Gunn, J. E., Ivezić, Z., Knapp, G. R., Kent, S. M., & Yasuda, N. 2001, in Proceedings of ADASS X, in press, astro-ph 0101420.

Lupton, R. H., Gunn, J. E., & Szalay, A. 1999, AJ, 118, 1406

Marcy, G. W., & Butler, R. P. 1998, in “Brown Dwarfs and Extrasolar Planets”, ed. R. Rebolo, E.L. Martín & M.R. Zapatero-Osorio, A.S.P. Conf. Ser. 134, 128

Marcy, G. W., & Butler, R. P. 2000, PASP, 112, 137

Marcy, G. W., Cochran, W. D., & Mayor, M. 2000, in Protostars and Planets IV, eds. V. Mannings, A. P. Boss, S. S. Russell (Tucson: Univ. Arizona Press), 1285

Marley, M. S., & Ackerman, A. J. 2001, in IAU Symposium 202, Planetary Systems in the Universe: Observation, Formation and Evolution, A.S.P. Conf. Ser., in press (astro-ph/0103269)

Martín, E. L., Basri, G., Delfosse, X., & Forveille, T. 1997, A&A, 327, L29

Martín, E. L., Brandner, W., & Basri, G. 1999, Science, 283, 718

Martín, E. L., Delfosse, X., Basri, G., Goldman, B., Forveille, T., & Zapatero-Osorio, M. R. 1999, AJ, 118, 2466 (M99)

Mayor, M. & Queloz, D. 1995, Nature, 378, 355

McLean, I. S., Graham, J. R., Becklin, E. E., Figer, D. F., Larkin, J. E., Levenson, N. A., & Teplitz, H. I. 2000a, Proc. SPIE 4008, 1048

McLean, I. S., et al. 2000b, ApJ, 533, L45

Mountain, C. M., Robertson, D., Lee, T. J., & Wade, R. 1990, Proc. SPIE, 1235, 25

Nakajima, T., Oppenheimer, B. R., Kulkarni, S. R., Golimowski, D. A., Matthews, K., & Durrance, S. T., 1995, Nature, 378, 463

Nakajima, T., Tsuji, T., Maihara, T., Iwamuro, F., Motohara, K., Taguchi, T., Hata, R., Tamura, M., & Yamashita, T. 2000, PASJ, 52, 87

Noll, K. S., Geballe, T. R., Leggett, S. K., & Marley, M. S. 2000, ApJ, 541, L75

Oppenheimer, B. R., Kulkarni, S. R., Matthews, K., & Nakajima, T. 1995, Science, 270, 1478

Oppenheimer, B. R., Kulkarni, S. R., Matthews, K., & van Kerkwijk, M. H. 1998, ApJ, 502, 932

Oke, J. B., & Gunn, J. E. 1983, ApJ, 266, 713

Pinfield, D. J., Hodgkin, S. T., Jameson, R. F., Cossburn, M. R., Hambly, N. C., & Devereux, N. 2000, MNRAS, 313, 347

Ramsey, L.W., et al. 1998, Proc. SPIE 3352, 324

Reid, I. N., et al. 1999, ApJ, 521, 613

Reid, I. N., 2001, in ‘Galactic Structure, Stars and the Interstellar Medium’, ed. C. Woodward & M. Bicay, ASP Conf Ser (in press - astro-ph/0010203)

Reid, I.N., Burgasser, A.J., Cruz, K.L., Kirkpatrick, J.D., & Gizis, J.E. 2001, AJ, 121, 1710

Reid, I. N., & Hawley, S. L. 2000, New Light on Dark Stars: Red Dwarfs, Low-Mass Stars, and Brown Dwarfs (New York: Springer-Praxis)

Ruiz, M. T., Leggett, S. K., & Allard, F. 1997, ApJ, 491, L107

Schneider, D.P., et al. 2002, AJ, in press

Skrutskie, M.F., et al. 1997, in The Impact of Large-Scale Near-IR Sky Surveys, ed. F. Garzon et al. (Dordrecht: Kluwer), 25

Strauss, M. A. et al. 1999, ApJ, 522, L61

Testi, L., et al. 2001, ApJ, 552, L147

Tinney, C. G., Delfosse, X., Forveille, T., & Allard, F. 1998, A&A, 338, 66

Tokunaga, A. T., & Kobayashi, N. 1999, AJ, 117, 1010

Tsuji, T. 2001, in ‘Proceedings of the Meeting on Ultracool Dwarfs’, I.A.U. 24th General Assembly, eds. H.R.A. Jones, M. Gerbaldi, & I.A. Steele (Heidelberg: Springer-Verlag), in press

Tsvetanov, Z. I., et al. 2000, ApJ, 531, L61

York, D. G., et al. 2000, AJ, 120, 1579

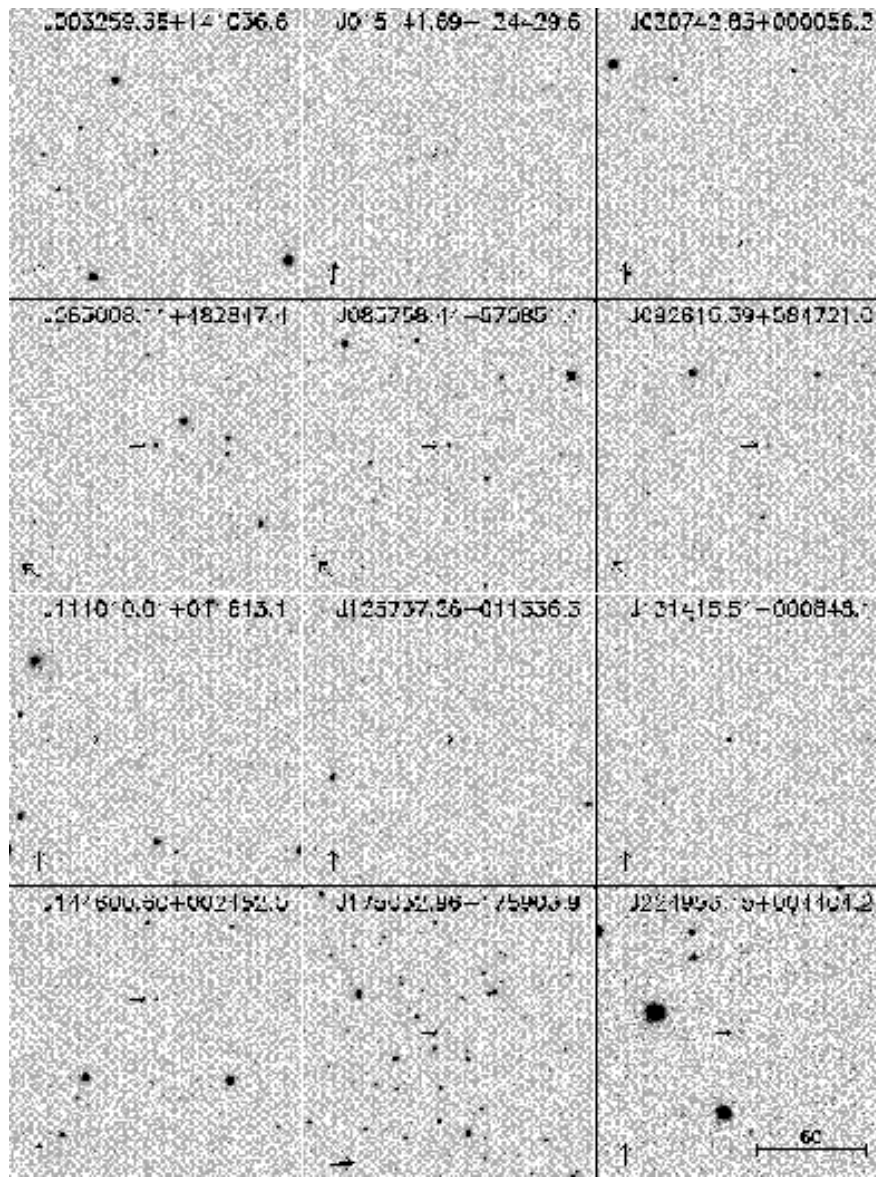


Fig. 1.— z finding charts for twelve new SDSS dwarfs. North is denoted by the arrow at bottom left of each chart; east is counterclockwise from north.

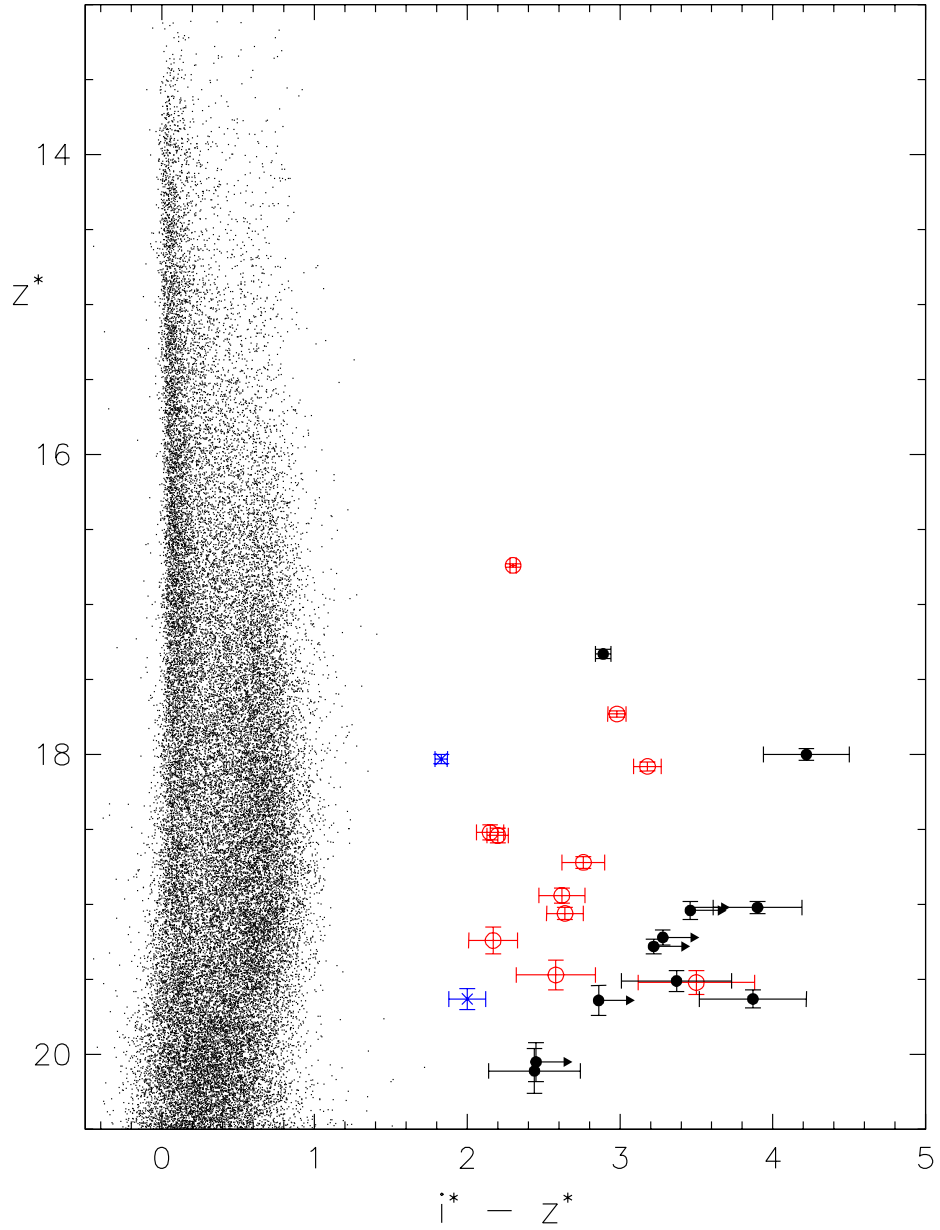


Fig. 2.— Color magnitude diagram, z^* vs. $i^* - z^*$, for low mass stars and substars selected from the SDSS imaging data and discussed in the present paper. For comparison, the data for a random sample of 50,000 high-latitude stars selected from the SDSS imaging data are shown - the objects in this sample were selected to be detected and point-like separately in the SDSS g , r and i band data. The symbols represent the spectral classes assigned in this paper. Crosses: M. Open: L. Filled: T. The lower limits to the $i^* - z^*$ colors are calculated assuming the 5σ limit of 22.5 magnitudes at i band. The error bars are 1σ , and do not contain a contribution for systematic zero-point error.

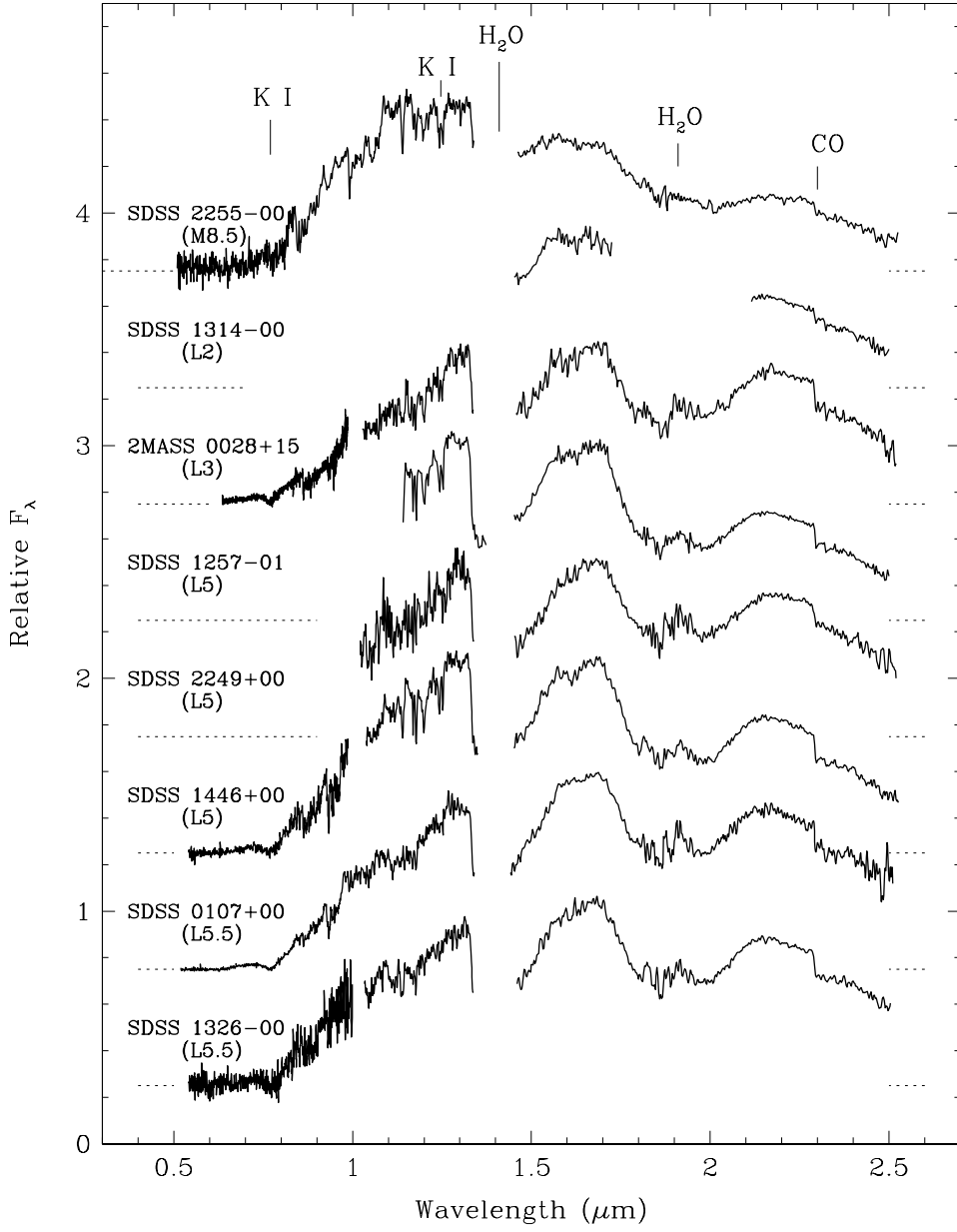


Fig. 3a.— New spectra of twenty-seven M, L, and T dwarfs. The SDSS or 2MASS identifications are each given above the dashed line which corresponds to the zero flux level for each spectrum. The complete catalogue names are given in Tables 1-3. The locations of significant spectral features are indicated at the top of each figure. Classifications are from this paper. Local noise can be judged by point-to-point variations. M9 through L5.5.

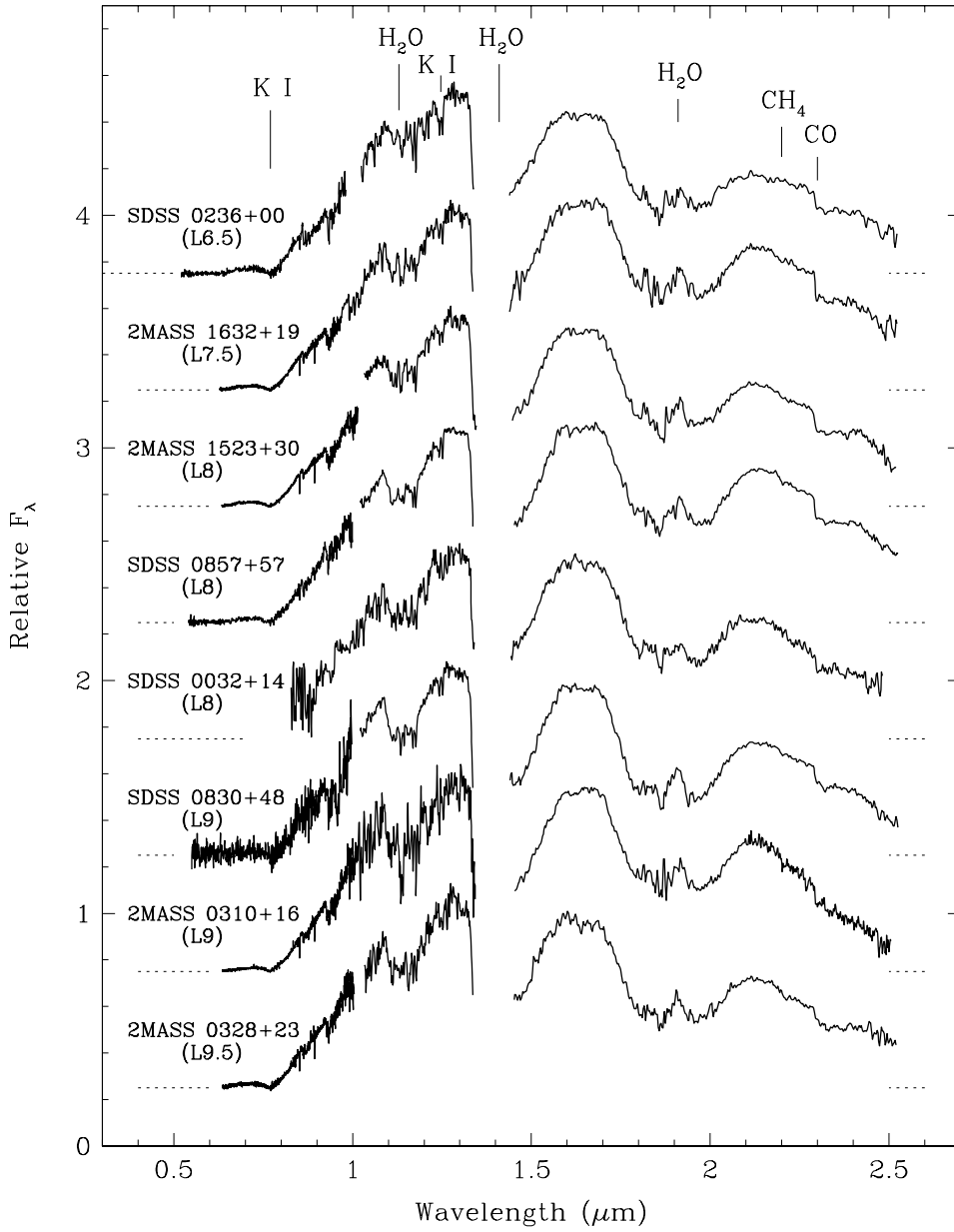


Fig. 3b.— L6.5 through L9. 2MASS 0310+16 includes our data (J and H), optical data from K00, and infrared data from R01 (K).

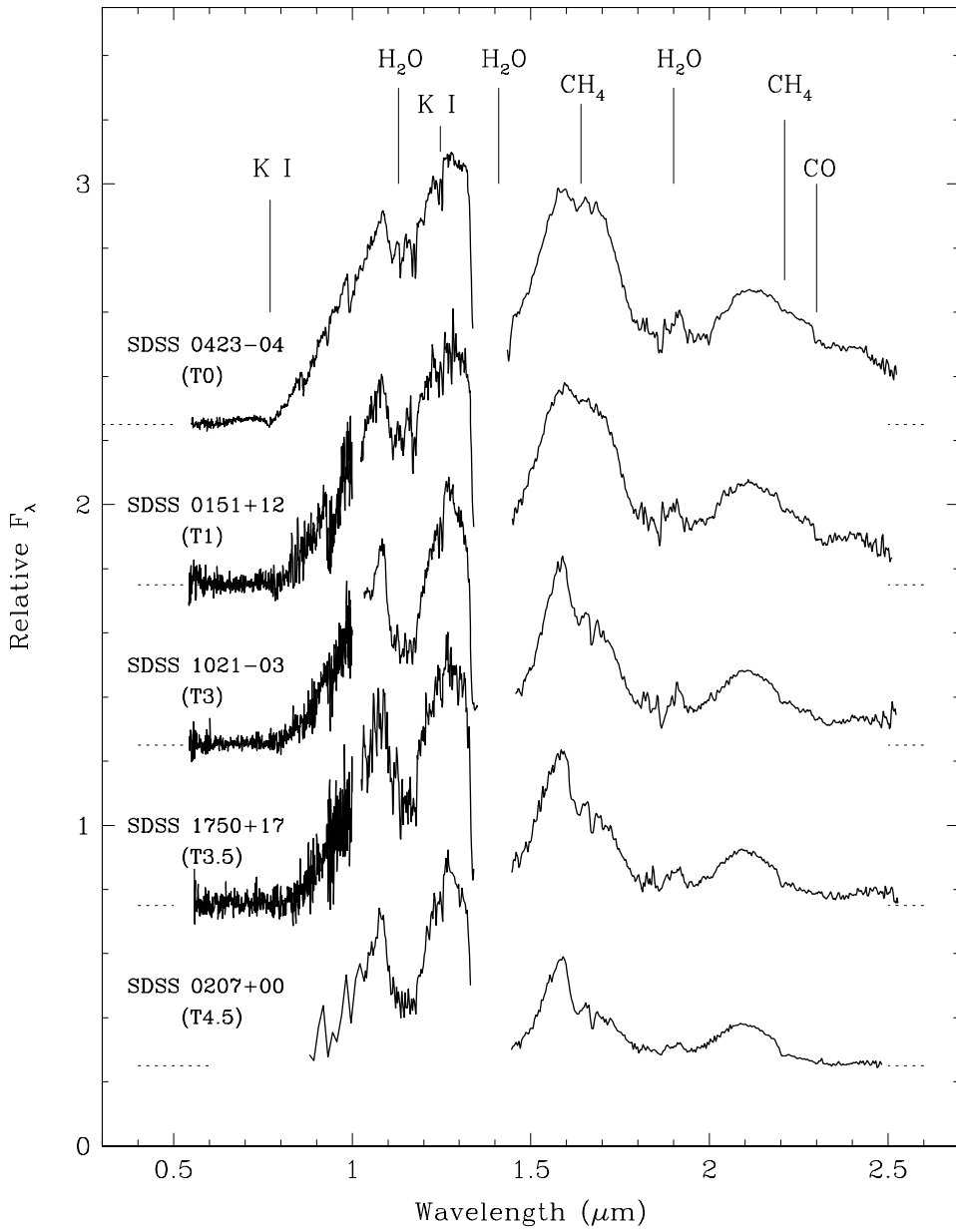


Fig. 3c.— T0 through T4.5.

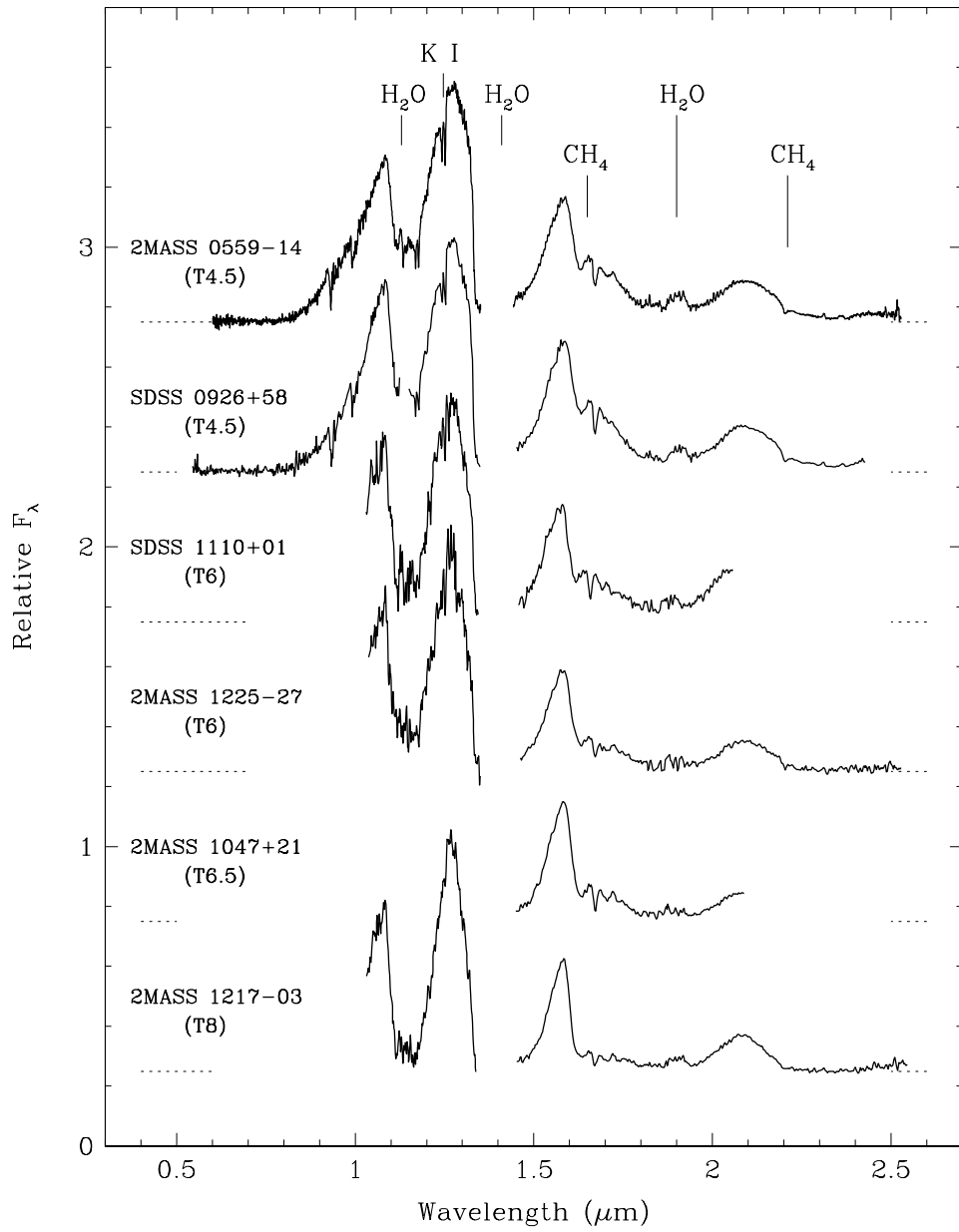


Fig. 3d.— T4.5 through T8.

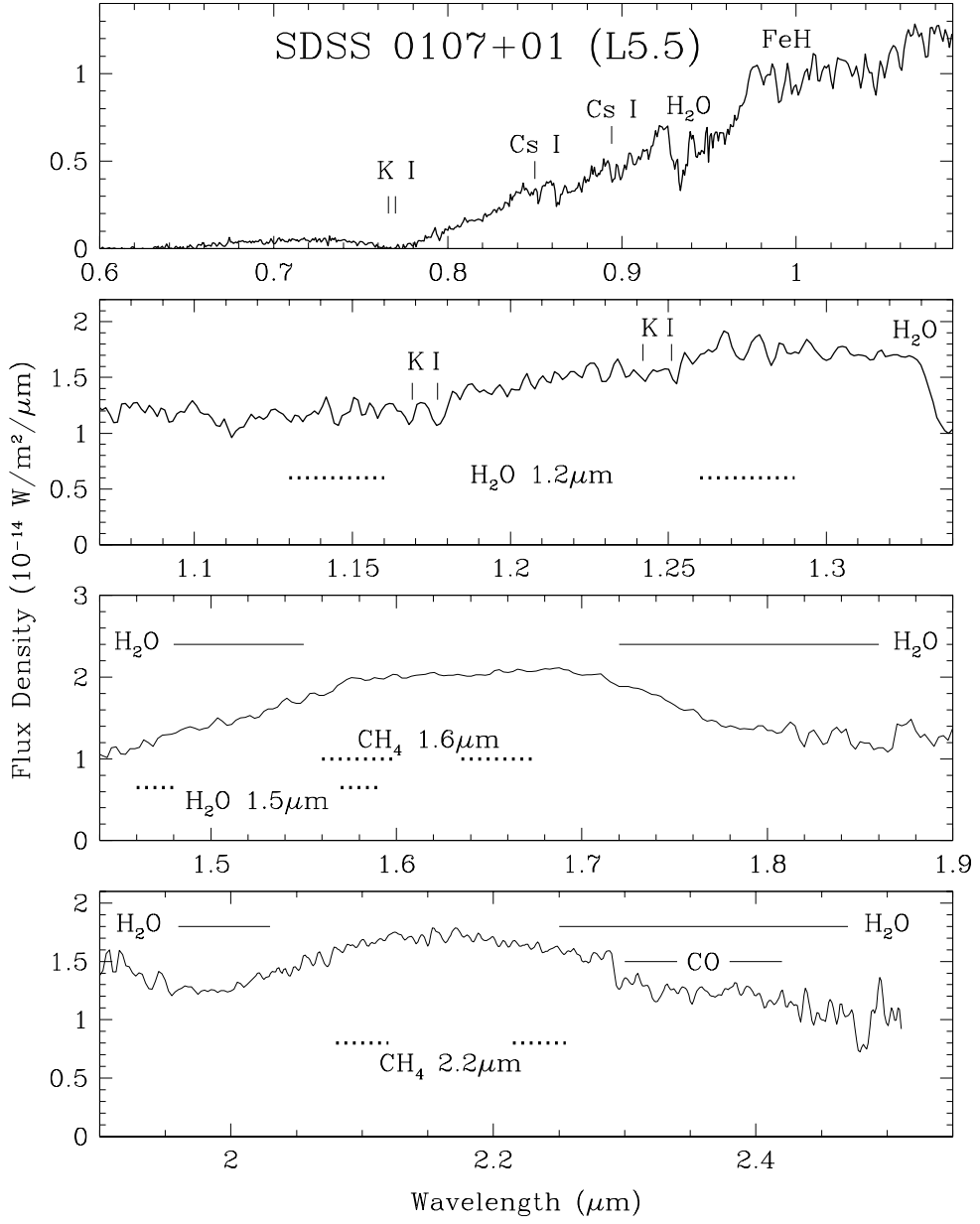


Fig. 4a.— Spectra of a mid-L dwarf and a mid-T dwarf from 0.6 to 2.5 μm . The wavelengths of prominent spectral lines and bands are marked, and the wavelength ranges where the water and methane indices are calculated are indicated by dotted lines. The L5.5 dwarf SDSS 0107+01.

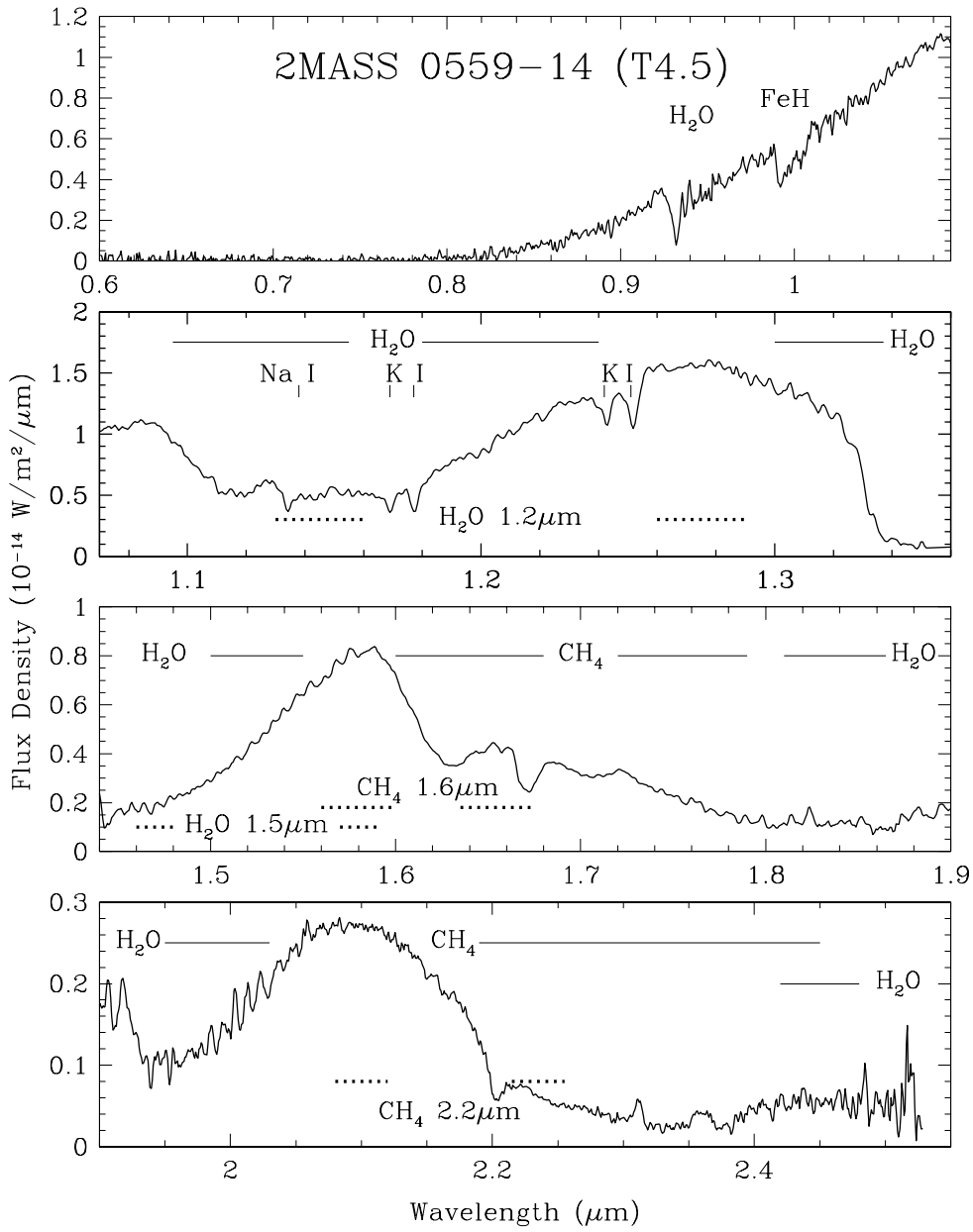


Fig. 4b.— The T4.5 dwarf 2MASS 0559-14.

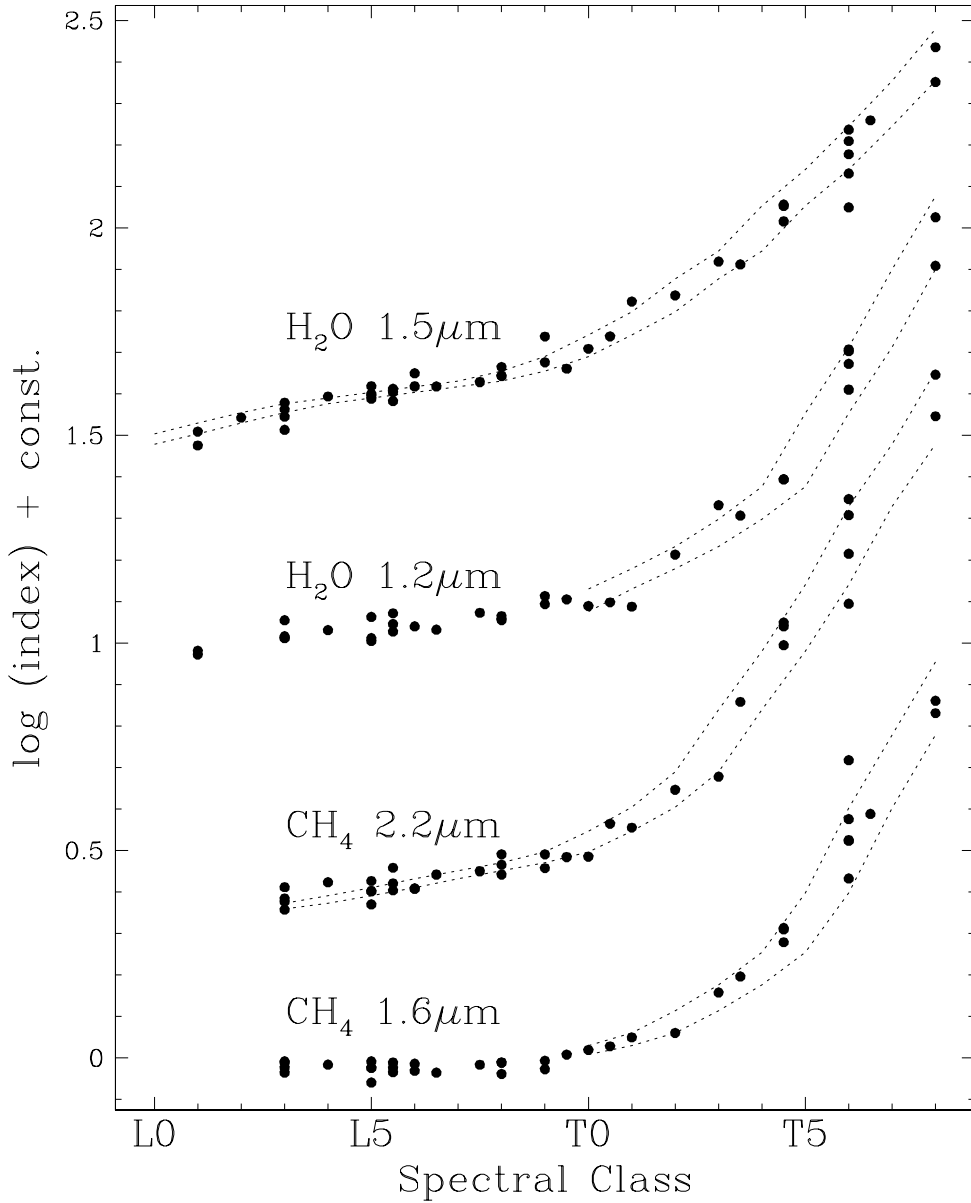


Fig. 5.— Index values versus final assigned spectral class for the four infrared indices. The space between the pairs of dashed lines denotes the range of values of the index for each spectral class, according to the definitions in Table 5.

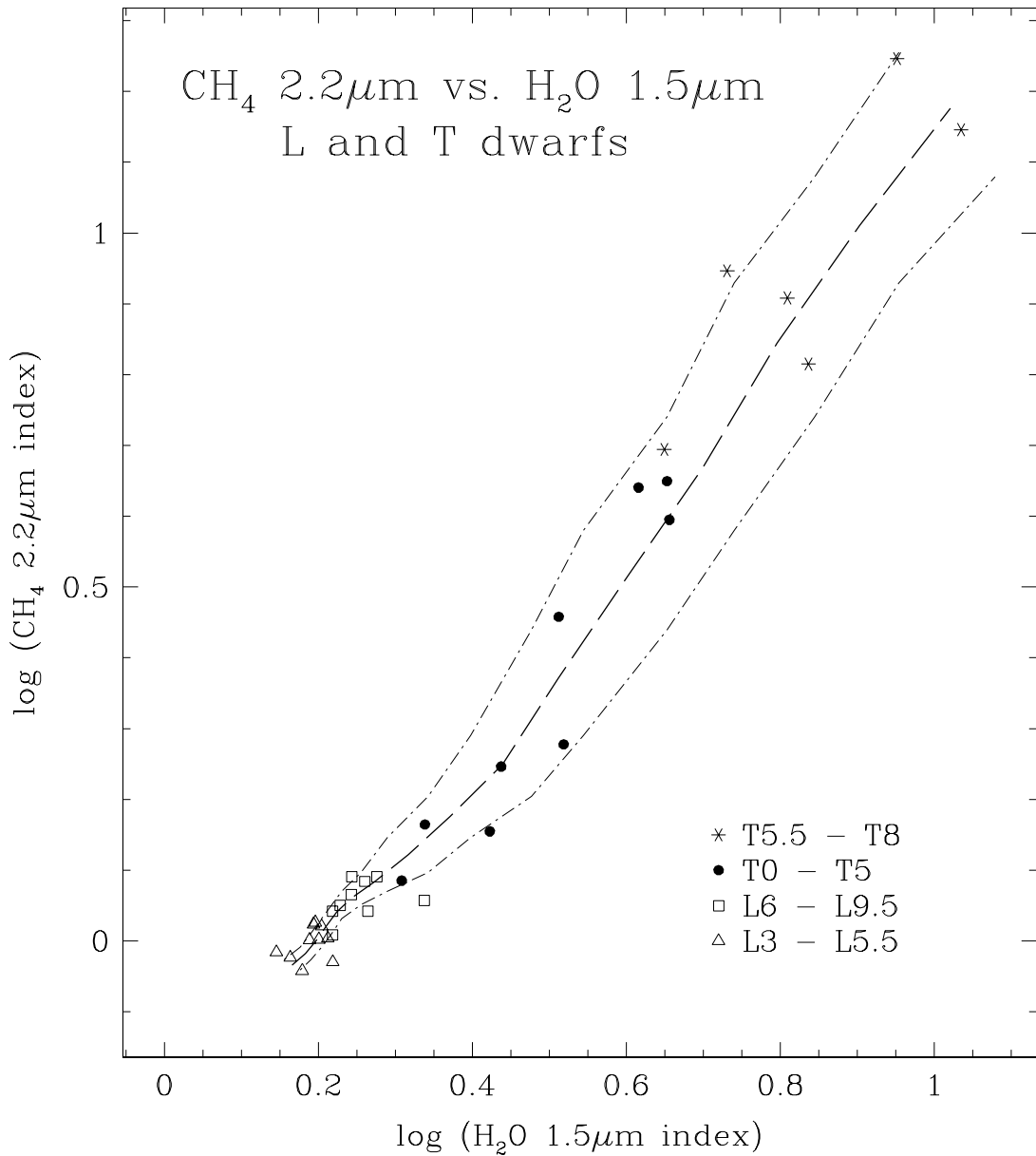


Fig. 6a.— The methane 2.2 μ m index plotted against the water 1.5 μ m index, for L and T spectral classes. The dashed line connects the mean values of the subclasses according to the definitions in Table 5; the dot-dashed lines differ from the mean by ± 1 subclass. L and T classes.

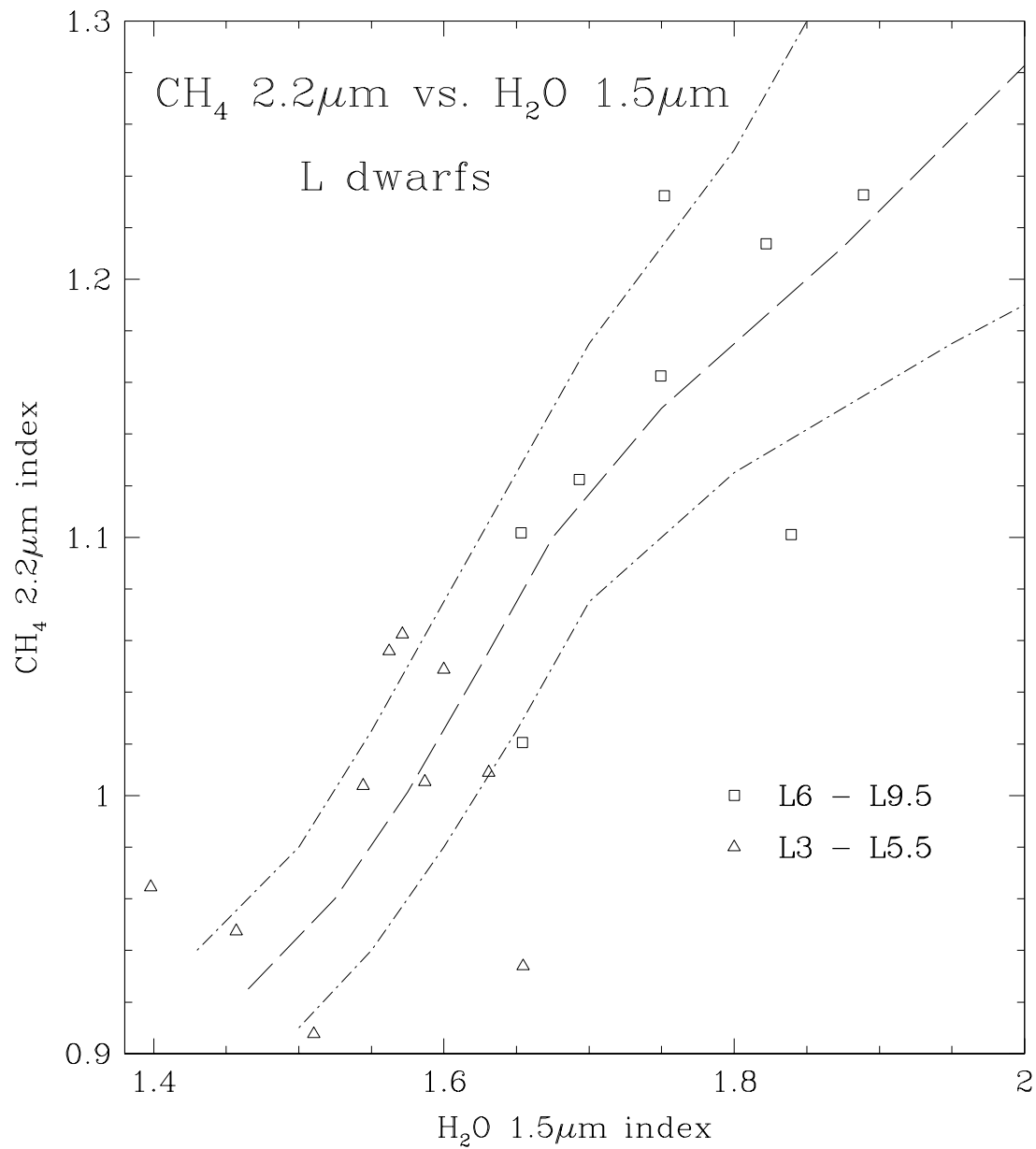


Fig. 6b.— L class only.

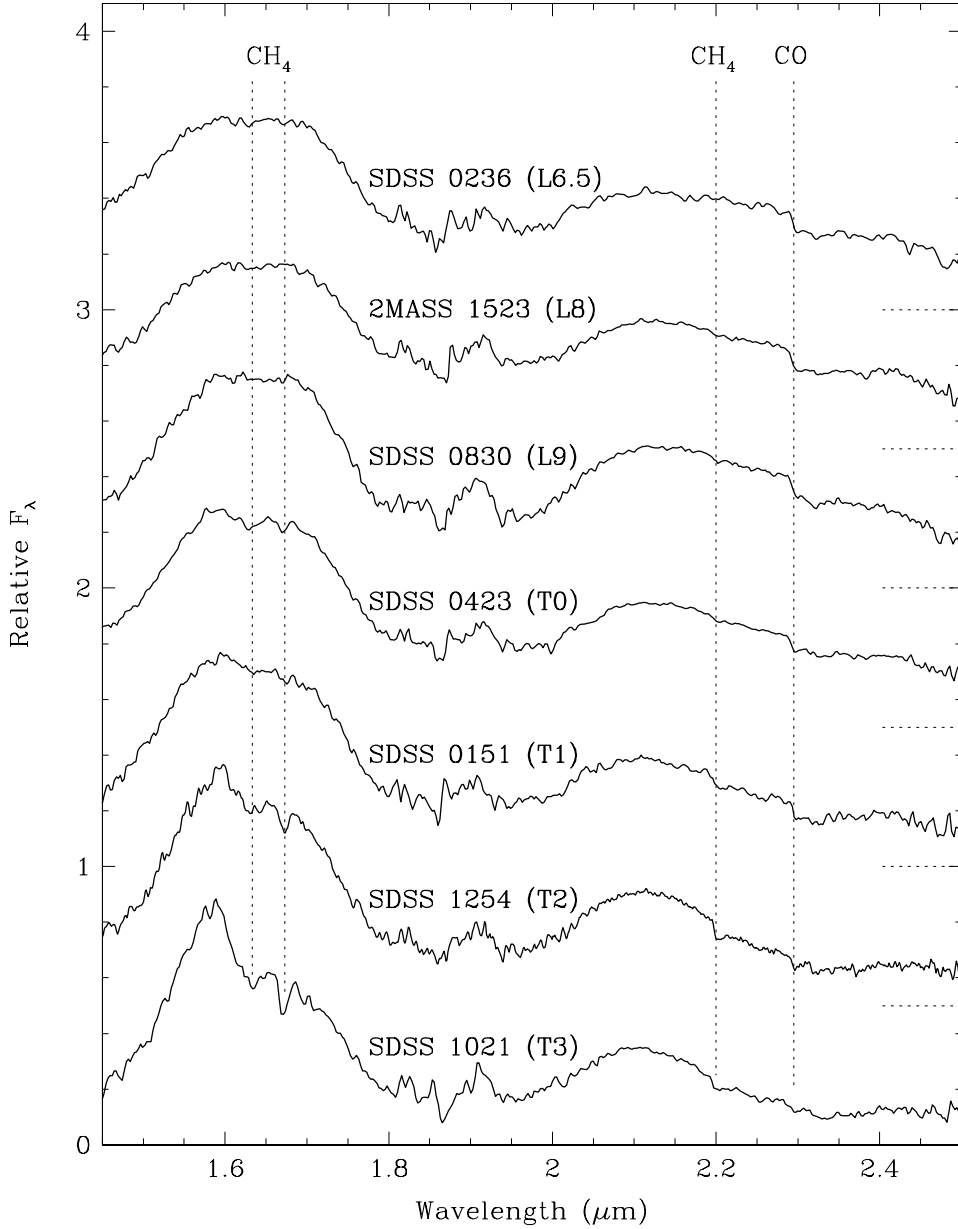


Fig. 7.— Spectra from 1.5 to 2.5 μ m of late L and early T dwarfs, showing the onset of absorption by methane in the H and K bands. Horizontal dashed lines below each spectrum indicate zero flux levels. Vertical dashed lines mark the wavelengths of spectral features due to CH_4 and CO. Classifications are from this paper. Spectrum of SDSS 1254-01 is from L00b.

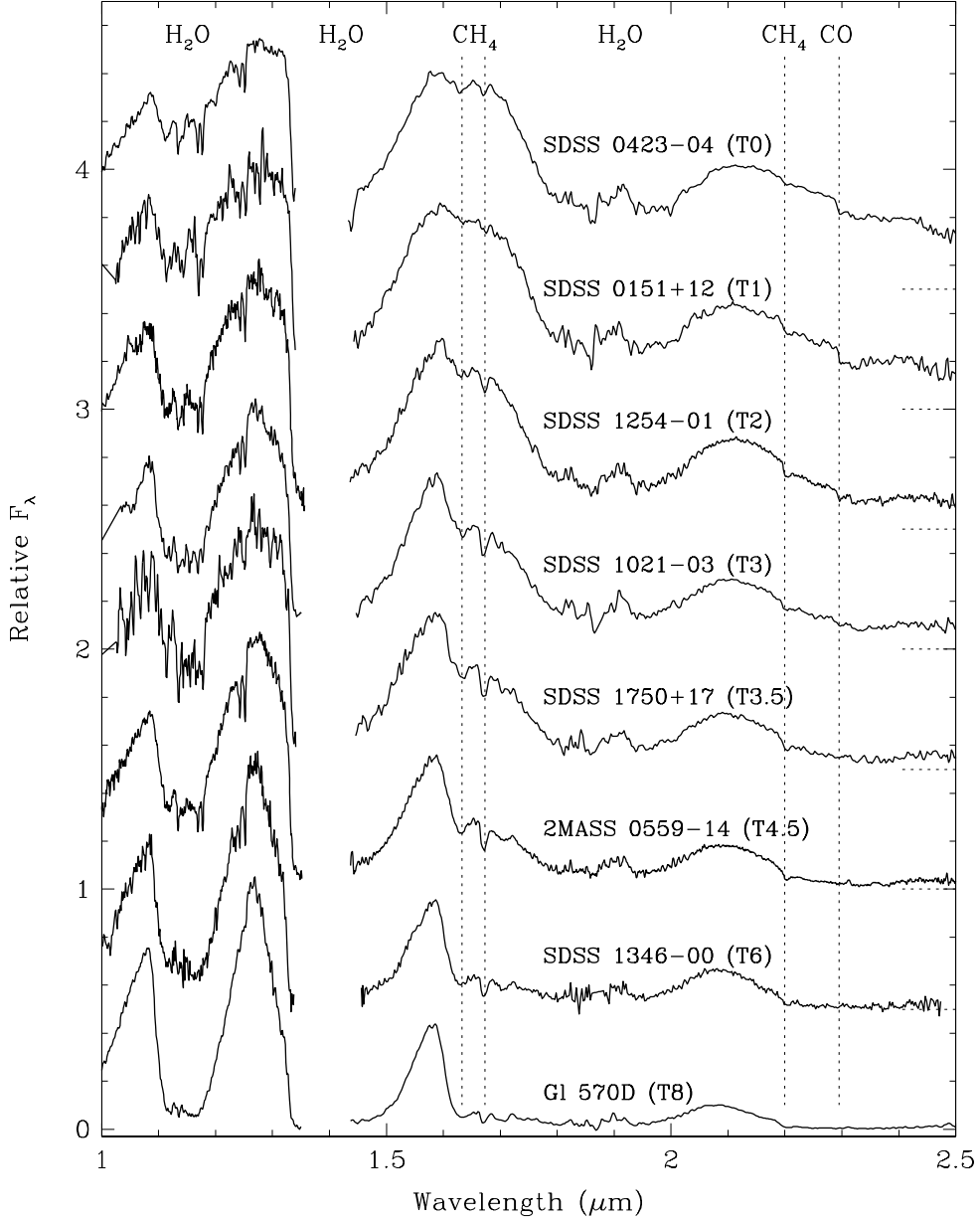


Fig. 8.— The T sequence from 1.0 to 2.5 μm . The spectra are normalized at their peaks near 1.3 μm . The wavelengths of broad water absorption bands are indicated. Vertical dashed lines mark the wavelengths of key spectral features due to CH_4 and CO . Classifications are from this paper. Spectra of SDSS 1254-01, SDSS1346-00, and GI 570D are from L00b, Tsvetanov et al. (2000), and Geballe et al. (2001a), respectively.

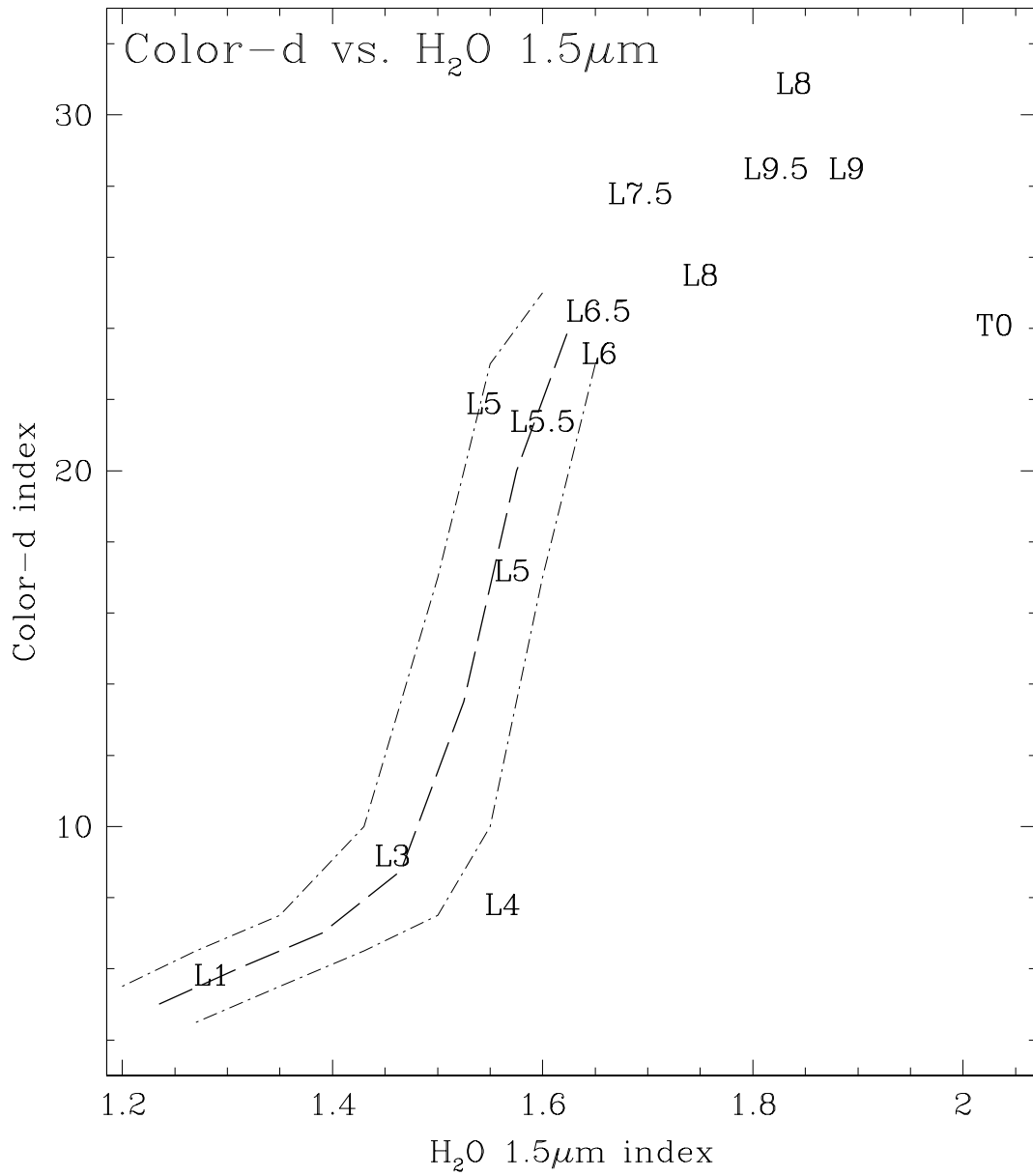


Fig. 9.— The modified 2MASS optical “Color-d” index plotted against the H₂O 1.5 μ m index for isolated L dwarfs and the T0 dwarf SDSS 0423-04. The dashed line connects the midpoints of the range of each subclass where both are defined; the dash-dot lines deviate by one subclass. Data points are from Table 4.

Table 1. Photometry of New SDSS Objects^{a,b,c}

Name ^d	<i>r</i> [*]	<i>i</i> [*]	<i>z</i> [*]	J-K	J-H	H-K	K
SDSSp J003259.36+141036.6	(24.18±0.56)	(23.02±0.37)	19.52±0.08	1.59±0.07	0.92±0.07	0.67±0.07	14.99±0.05
SDSSp J010752.33+004156.1	(23.81±0.53)	21.48±0.13	18.72±0.04	2.17±0.04	1.19±0.04	0.98±0.04	13.58±0.03
SDSSp J015141.69+124429.6	(24.12±0.55)	(22.88±0.35)	19.51±0.07	1.07±0.07	0.71±0.07	0.36±0.07	15.18±0.05
SDSSp J020742.83+000056.2	(23.90±0.49)	22.55±0.26	20.11±0.15	0.01±0.07	-0.03±0.07	0.04±0.07	16.62±0.05
SDSSp J023617.93+004855.0	(24.53±0.58)	21.56±0.14	18.94±0.05	1.47±0.07	0.85±0.07	0.62±0.07	14.54±0.05
SDSSp J042348.57-041403.5	22.64±0.20	20.22±0.04	17.33±0.03	1.34±0.04	0.79±0.04	0.55±0.04	12.96±0.03
SDSSp J083008.12+482847.4	(23.59±0.48)	21.26±0.08	18.08±0.03	1.54±0.04	0.82±0.04	0.72±0.04	13.68±0.03
SDSSp J085758.45+570851.4	23.02±0.30	20.71±0.06	17.73±0.02	1.86±0.04	1.00±0.04	0.86±0.04	12.94±0.03
SDSSp J092615.38+584720.9	(24.96±0.88)	(24.29±1.03)	19.04±0.06	-0.03±0.04	0.05±0.04	-0.08±0.04	15.50±0.03
SDSSp J111010.01+011613.1		(23.98±0.82)	19.64±0.10	0.07±0.07	-0.10±0.07	0.17±0.07	16.05±0.05
SDSSp J125737.26-011336.1	22.71±0.27	20.67±0.08	18.52±0.05	1.58±0.04	0.96±0.04	0.62±0.04	14.06±0.03
SDSSp J131415.52-000848.1	(23.32±0.28)	21.63±0.10	19.63±0.07	1.05±0.07	0.49±0.07	0.56±0.07	15.28±0.05
SDSSp J144600.60+002452.0	(23.35±0.29)	20.74±0.05	18.54±0.05	1.76±0.07	0.97±0.07	0.79±0.07	13.80±0.05
SDSSp J175032.96+175903.9	(24.89±0.47)	(23.50±0.35)	19.63±0.06	0.12±0.07	0.20±0.07	-0.08±0.07	16.02±0.05
SDSSp J224953.45+004404.2	(23.88±0.57)	22.05±0.24	19.47±0.10	2.03±0.07	1.04±0.07	0.99±0.07	14.43±0.05
SDSSp J225529.09-003433.4	22.23±0.16	19.86±0.03	18.03±0.03	1.22±0.07	0.70±0.07	0.52±0.07	14.28±0.05

^aThe SDSS photometry is reported in asinh magnitudes (Lupton, Gunn, & Szalay 1999). Zero flux corresponds to $z^*=24.8$, $i^*=24.4$ and $z^*=22.8$. Values in parentheses are less than 5 σ detections.

^bThe SDSS magnitudes are AB_ν (Fukugita et al 1996) and the UKIRT magnitudes are on the Vega system.

^cUKIRT (JHK) photometry is on the MKO system.

^dThe ‘p’ in SDSSp stands for “preliminary astrometry.” Coordinates are J2000.

Table 2. Optical Spectroscopy

Name	Telescope/ Spectrograph	Date
SDSSp J010752.33+004156.1	HET/LRS	10/16/1999
SDSSp J015141.69+124429.6	ARC/DIS	09/02/2000
SDSSp J023617.93+004855.0	HET/LRS	10/06/1999
SDSSp J042348.57-041403.5	ARC/DIS	01/19/2001
2MASSW J055919.1-140448	ARC/DIS	12/20/2000
SDSSp J083008.12+482847.4	ARC/DIS	01/19/2001
SDSSp J085758.45+570851.4	ARC/DIS	02/02/2001
SDSSp J092615.38+584720.9	ARC/DIS	01/19/2001
SDSSp J102109.69-030420.1	ARC/DIS	02/02/2001
SDSSp J144600.60+002452.0	ARC/DIS	03/01/2000
SDSSp J175032.96+175903.9	ARC/DIS	02/02/2001
SDSSp 225529.09-003433.4	HET/LRS	12/07/1999

Table 3. Infrared Spectra: Observations

Name	Telescope/ Spectrograph	Bands	Date
2MASSI J002839.44+150141.8	UKIRT/CGS4	J	10/13/2000
	UKIRT/CGS4	H,K	12/06/2000
	Keck/NIRSPEC	J _s	12/23/2000
SDSSp J003259.36+141036.6	UKIRT/CGS4	Z,J,H,K	09/20-23/2000
SDSSp J010752.33+004156.1	UKIRT/CGS4	J,H,K	09/20-23/2000
SDSSp J015141.69+124429.6	UKIRT/CGS4	J,H,K	09/20-23/2000
SDSSp J020742.83+000056.2	IRTF/NSFCAM	Z	09/23/2000
	UKIRT/CGS4	J	12/07/2000
	Keck/NIRSPEC	H,HK,K	12/22-23/2000
SDSSp J023617.93+004855.0	UKIRT/CGS4	J,H,K	09/20-23/2000
2MASSW J031059.9+164816	UKIRT/CGS4	J	07/12/2001
	UKIRT/CGS4	H	07/18/2001
2MASSW J032842.6+230205	UKIRT/CGS4	J,H,K	12/05-07/2000
SDSSp J042348.57-041403.5	UKIRT/CGS4	Z,J,H,K	09/20-23/2000
2MASSW J055919.1-140448	UKIRT/CGS4	J,H,K	09/20-23/2000
	UKIRT/CGS4	Z,J	12/05-07/2000
SDSSp J083008.12+482847.4	UKIRT/CGS4	J,H,K	12/05-07/2000
SDSSp J085758.45+570851.4	UKIRT/CGS4	J,H,K	12/05-07/2000
SDSSp J092615.38+584720.9	Keck/NIRSPEC	J _s ,J,H,HK,K	12/21-23/2000
SDSSp J102109.69-030420.1	Keck/NIRSPEC	J _s	12/22/2000
2MASSI J104753.9+212423	UKIRT/CGS4	H	05/21/2001
SDSSp J111010.01+011613.1	UKIRT/CGS4	H	05/21/2001
	UKIRT/CGS4	J	5/24/2001
2MASSW J121711.1-031113	UKIRT/CGS4	H	05/21/2001
	UKIRT/CGS4	J,K	5/24/2001
2MASSW J1225543-273947	UKIRT/CGS4	H	06/16/2001
	UKIRT/CGS4	J	07/12/2001
	UKIRT/CGS4	K	07/18/2001
SDSSp J125737.26-011336.1	Keck/NIRSPEC	J,H,HK,K	12/22-23/2000
SDSSp J131415.52-000848.1	Keck/NIRSPEC	H,K	12/23/2000
SDSSp J132629.82-003831.5	UKIRT/CGS4	J,H,K	03/13-15/2000
SDSSp J144600.60+002452.0	UKIRT/CGS4	J,H,K	03/13-15/2000
2MASSW J152322.6+301456	UKIRT/CGS4	J,H,K	03/13-15/2000
2MASSW J163229.1+190441	UKIRT/CGS4	Z,J,H,K	09/20-23/2000
SDSSp J175032.96+175903.9	UKIRT/CGS4	J,H	02/19/2001
	UKIRT/CGS4	K	05/06/2001
SDSSp J224953.45+004404.2	UKIRT/CGS4	J,H,K	12/05-07/2000
	Keck/NIRSPEC	J _s	12/23/2000
SDSSp J225529.09-003433.4	UKIRT/CGS4	J,H,K	09/20-23/2000

Table 4. Spectral Indices^a and Classifications of Cool Dwarfs

Name	PC3 ^b	Color-d ^c	Cont 1.0 μ m	H ₂ O 1.2 μ m	H ₂ O 1.5 μ m	CH ₄ 1.6 μ m	H ₂ O 2.0 μ m	CH ₄ 2.2 μ m	Assigned Class ^d
	0.823–0.827/ 0.754–0.758	0.96–0.98/ 0.735–0.755	1.04–1.05/ 0.875–0.885	1.26–1.29/ 1.13–1.16	1.57–1.59/ 1.46–1.48	1.56–1.60/ 1.635–1.675	2.09–2.11/ 1.975–1.995	2.08–2.12/ 2.215–2.255	
LHS 65	...	0.85	...	0.82	0.91	...	M1
LHS 38	0.96	0.47	0.97	0.84	0.96	...	M1
LHS 386	1.03	0.93	0.42	0.87	0.94	...	M1
LHS 443	0.99	...	0.94	...	M1.5
LHS 399	0.98	...	0.97	...	M2.5
LHS 502	0.94	...	0.97	...	M2.5
LHS 5327	0.81	0.93	0.91	...	0.96	...	M3
LHS 54	1.03	...	0.96	...	M3
LHS 58	1.00	...	0.95	0.87	0.90	...	0.92	...	M3
LHS 2945	1.11	1.21	1.07	0.93	0.94	...	0.97	...	M3.5
LHS 4	0.96	1.15	0.95	1.01	1.00	...	0.98	...	M3.5
LHS 427	1.00	1.06	...	0.96	...	M3.5
LHS 59	1.12	0.97	...	0.94	...	M3.5
LHS 57	1.12	1.35	0.92	0.95	0.99	...	M4
LHS 3509	0.97	...	1.01	...	M4.5
LHS 400	1.03	...	1.04	...	M4.5
LHS 421	1.17	1.24	0.92	0.91	1.08	...	0.95	...	M4.5
LHS 3494	1.19	1.87	1.27	0.98	1.04	...	1.05	...	M5.5
LHS 2	...	2.20	1.40	0.92	0.99	...	M5.5
LHS 3406	1.68	0.94	1.08	...	1.08	...	M5.5
LHS 39	1.32	1.81	1.35	1.05	1.04	...	1.04	...	M5.5
LHS 330	1.42	1.08	...	1.03	...	M6
LHS 3339	1.42	1.04	1.02	...	1.00	...	M6
LHS 3495	1.37	0.92	1.01	...	1.01	...	M6
LHS 36	1.62	2.5	...	1.00	1.03	...	1.04	...	M6
LHS 5328	1.26	1.03	1.02	...	1.04	...	M6
LHS 292	1.58	0.97	1.04	...	M6.5
LHS 2930	1.68	2.9	1.85	1.00	1.16	...	1.07	...	M6.5
LHS 523	1.58	...	1.45	0.96	1.01	...	1.04	...	M6.5
LHS 429	1.51	2.4	1.61	1.03	1.06	...	M7
LHS 3003	1.67	1.12	1.17	...	1.09	...	M7
T 513	1.99	...	2.8	1.09	1.05	...	1.09	...	M8.5
SDSS 2255-00	2.2	1.00	1.15	...	1.12	...	M8.5
LHS 2065	1.95	1.15	1.15	...	1.11	...	M9
LP 944	2.5	1.19	1.25	...	1.13	...	M9
BRI 0021	2.3	4.7	...	1.22	1.24	...	1.15	...	M9.5
2MASS 0345+25	3.2 (L2.5)	1.20	1.19 (<L0)	...	1.09	...	L1±1
2MASS 0746+20	2.7 (L1)	5.8 (L1)	2.2	1.18	1.29 (L1)	...	1.21	...	L1
SDSS 1314-00	1.39 (L2)	L2(?)
Kelu-1	2.9 (L2.5)	...	4.1	1.31	1.40 (L2)	0.98	1.27	0.96 (L4)	L3±1
GD 165B	3.5 (L3)	8.8 (L3)	3.9	1.30	1.30 (L1)	0.98	1.36	1.03 (L5.5)	L3±2
DENIS 1058-15	3.5 (L3)	7.4 (L2.5)	3.5	1.29	1.51 (L3.5)	0.95	...	0.91 (L3)	L3
2MASS 0028+15	4.0 (L3)	9.2 (L3)	3.4	1.43	1.46 (L3)	0.92	1.36	0.95 (L4)	L3
2MASS 0036+18	3.8 (L3)	7.8 (L2.5)	3.4	1.35	1.56 (L4.5)	0.96	1.29	1.06 (L5)	L4±1
SDSS 2249+00	1.45	1.65 (L6.5)	0.87	1.29	0.93 (L3)	L5±1
SDSS 1446+00	7.0	22. (L5.5)	3.1	1.27	1.54 (L4.5)	0.95	1.39	1.01 (L5)	L5
SDSS 1257-01	1.59 (L5.5)	0.95	1.44	1.01 (L5)	L5
SDSS 0539-00	8.5	17.2 (L4.5)	3.0	1.29	1.57 (L5)	0.98	1.43	1.06 (L6)	L5
SDSS 0107+00	6.4	21. (L5)	2.2	1.48	1.60 (L5.5)	0.95	1.41	1.05 (L6)	L5.5
SDSS 1326-00	1.40	1.63 (L6)	0.92	1.26	1.01 (L5)	L5.5
DENIS 0205-11	11.1	15.2 (L4)	3.3	1.34	1.52 (L4)	0.97	1.51	1.14 (L8)	L5.5±2
DENIS 1228-15	6.7	14.1 (L4)	4.0	1.38	1.78 (L8.5)	0.97	1.39	1.01 (L5)	L6±2
2MASS 0825+21	10.8	23. (L5.5)	3.2	...	1.65 (L6.5)	0.93	1.44	1.02 (L5.5)	L6
SDSS 0236+00	13.5	25. (L6.5)	3.2	1.35	1.65 (L6.5)	0.92	1.49	1.10 (L7)	L6.5
2MASS 1632+19	12.3	28.	2.5	1.49	1.69 (L7.5)	0.96	1.45	1.12 (L7.5)	L7.5
2MASS 1523+30	11.7	25. (L6.5)	2.9	1.43	1.75 (L8)	0.97	1.42	1.16 (L8)	L8
SDSS 0857+57	17.5	31.	2.7	1.44	1.84 (L9)	0.97	1.49	1.10 (L7)	L8±1
SDSS 0032+14	1.46	1.75 (L8)	0.92	1.48	1.23 (L8.5)	L8
SDSS 0830+48	1.56 (T0)	2.18 (T0.5)	0.98 (<T0)	1.91	1.14 (L8)	L9±1
2MASS 0310+16	8.1	29.	2.8	1.63 (T0)	1.89 (L9)	0.94 (<T0)	1.19	1.23 (L9)	L9
2MASS 0328+23	9.6	29.	2.5	1.60 (T0)	1.82 (L8.5)	1.02 (L9.5)	1.55	1.21 (L9)	L9.5±1
SDSS 0423-04	7.1	24.	3.0	1.54 (T0)	2.03 (T0)	1.05 (T0)	1.51	1.22 (L9)	T0
SDSS 0837-00	...	19.8	4.5	1.58 (T0)	2.18 (T0.5)	1.07 (T0.5)	1.67	1.46 (T1)	T0.5
SDSS 0151+12	7.8	28.	3.1	1.54 (L9.5)	2.65 (T2)	1.12 (T1)	1.53	1.43 (T0.5)	T1±1
SDSS 1254-01	6.5	2.06 (T2)	2.74 (T2)	1.15 (T1.5)	1.83	1.76 (T2)	T2
SDSS 1021-03	4.3	2.70 (T4)	3.3 (T3)	1.44 (T3)	1.78	1.90 (T2.5)	T3
SDSS 1750+17	4.7	2.55 (T3.5)	3.3 (T3)	1.57 (T4)	2.00	2.87 (T3.5)	T3.5
SDSS 0926+58	7.9	...	4.5 (T4.5)	2.04 (T5)	2.13	3.9 (T4.5)	T4.5

Table 4—Continued

Name	PC3 ^b	Color-d ^c	Cont 1.0 μ m	H ₂ O 1.2 μ m	H ₂ O 1.5 μ m	CH ₄ 1.6 μ m	H ₂ O 2.0 μ m	CH ₄ 2.2 μ m	Assigned Class ^d
	0.823–0.827/	0.96–0.98/	1.04–1.05/	1.26–1.29/	1.57–1.59/	1.56–1.60/	2.09–2.11/	2.08–2.12/	
	0.754–0.758	0.735–0.755	0.875–0.885	1.13–1.16	1.46–1.48	1.635–1.675	1.975–1.995	2.215–2.255	
SDSS 0207+00	3.1 (T4.5)	4.5 (T4.5)	1.90 (T4.5)	2.08	4.5 (T5)	T4.5
2MASS 0559-14	3.5	88.	6.7	3.1 (T4.5)	4.1 (T4)	2.06 (T5)	2.11	4.4 (T5)	T4.5
G1 229B	15.5	6.4 (T6.5)	4.6 (T4.5)	5.2 (T7)	2.45	4.9 (T5)	T6±1
SDSS 1110+01	5.1 (T6)	6.0 (T6)	2.71 (T6)	T6
2MASS 1225-27	5.0 (T6)	6.4 (T6)	3.3 (T6)	2.50	8.1 (T6)	T6
SDSS 1346-00	6.1	5.9 (T6)	5.4 (T5.5)	3.8 (T6)	2.38	8.8 (T6.5)	T6
SDSS 1624+00	15.1	83.	7.7	6.4 (T6.5)	6.9 (T6.5)	3.4 (T6)	2.17	6.5 (T6)	T6
2MASS 1047+21	7.2 (T6.5)	3.9 (T6.5)	T6.5
2MASS 1217-03	10.2 (T7.5)	8.9 (T7.5)	6.8 (T8)	2.71	17.6 (T8.5)	T8
G1 570D	21.	13.3 (T8)	10.8 (T8)	7.2 (T8)	2.29	14.0 (T8)	T8

^aIndices are defined in Table 5 and discussed in Section 4.2.

^bIndex defined by M99 and discussed in Section 4.2.

^cIndex modified from the original definition (K99), as discussed in Section 4.2.

^dUncertainties are typically ± 0.5 , except where noted.

Table 5. Values of Indices^a for L and T Subtyping

Name	PC3 ^b [0.823–0.827]/ [0.754–0.758]	Color-d ^c [0.96–0.98]/ [0.735–0.755]	H ₂ O 1.2 μ m [1.26–1.29]/ [1.13–1.16]	H ₂ O 1.5 μ m [1.57–1.59]/ [1.46–1.48]	CH ₄ 1.6 μ m [1.56–1.60]/ [1.635–1.675]	CH ₄ 2.2 μ m [2.08–2.12]/ [2.215–2.255]
L0	2.4–2.6	4.5–5.5		1.20–1.27		
L1	2.6–2.85	5.5–6.5		1.27–1.35		
L2	2.85–3.25	6.5–7.5		1.35–1.43		
L3	3.25–4.25	7.5–10.		1.43–1.50		0.91–0.94
L4	4.25–6.0	10–17		1.50–1.55		0.94–0.98
L5		17–23		1.55–1.60		0.98–1.025
L6		23–25		1.60–1.65		1.025–1.075
L7				1.65–1.70		1.075–1.125
L8				1.70–1.80		1.125–1.175
L9				1.80–1.95		1.175–1.25
T0		1.5–1.7	1.95–2.2	1.02–1.07		1.25–1.40
T1		1.7–1.9	2.2–2.5	1.07–1.15		1.40–1.60
T2		1.9–2.15	2.5–3.0	1.15–1.30		1.60–1.95
T3		2.15–2.5	3.0–3.5	1.30–1.50		1.95–2.75
T4		2.5–3.0	3.5–4.5	1.50–1.80		2.75–3.8
T5		3.0–4.5	4.5–5.5	1.80–2.50		3.8–5.5
T6		4.5–6.5	5.5–7.0	2.5–4.0		5.5–8.5
T7		6.5–10.	7.0–9.0	4.0–6.0		8.5–12.
T8		10.–15.(?)	9.0–12.(?)	6.0–9.0(?)		12.–18.(?)

^aIndices are discussed in Section 4.2.

^bIndex defined by M99 and discussed in Section 4.2.

^cIndex modified from the original definition (K99), as discussed in Section 4.2.